

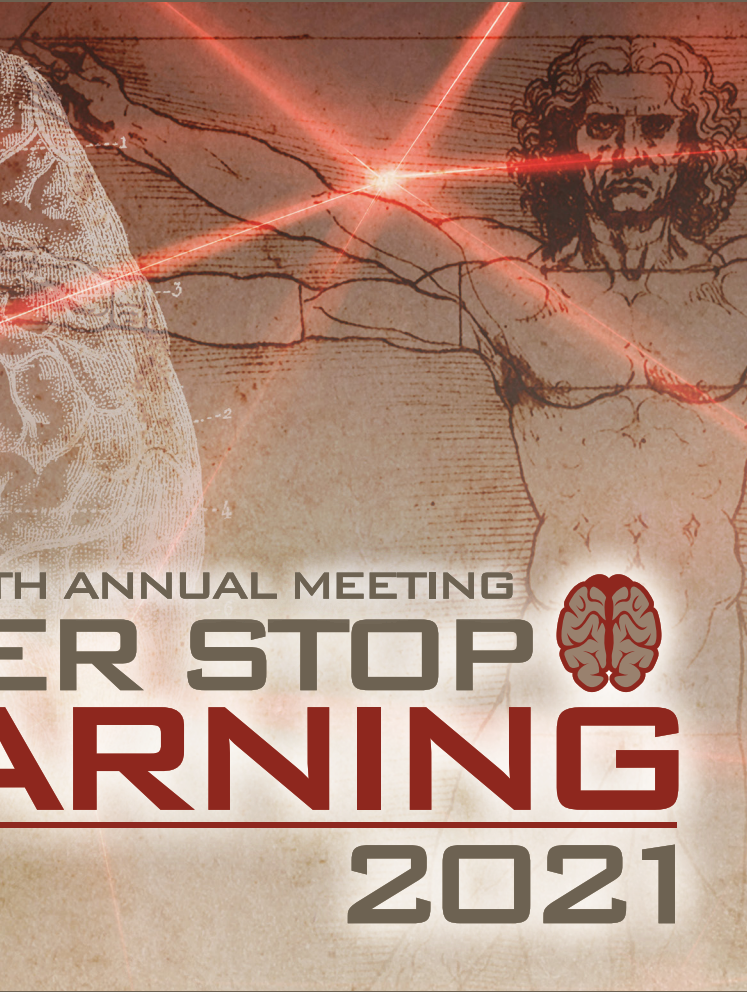
LI

LABORATORY INVESTIGATION

THE BASIC AND TRANSLATIONAL PATHOLOGY RESEARCH JOURNAL

ABSTRACTS

DERMATOPATHOLOGY (238-270)



USCAP 110TH ANNUAL MEETING
**NEVER STOP
LEARNING**
2021

MARCH 13-18, 2021

VIRTUAL AND INTERACTIVE

Published by
SPRINGER NATURE
www.ModernPathology.org

 **USCAP** AN OFFICIAL JOURNAL OF THE
UNITED STATES AND CANADIAN
ACADEMY OF PATHOLOGY
Creating a Better Pathologist

EDUCATION COMMITTEE

Jason L. Hornick
Chair

Rhonda K. Yantiss, Chair
Abstract Review Board and Assignment Committee

Kristin C. Jensen
Chair, CME Subcommittee

Laura C. Collins
Interactive Microscopy Subcommittee

Raja R. Seethala
Short Course Coordinator

Ilan Weinreb
Subcommittee for Unique Live Course Offerings

David B. Kaminsky
(Ex-Officio)
Zubair W. Baloch
Daniel J. Brat
Sarah M. Dry
William C. Faquin
Yuri Fedoriw
Karen Fritchie
Jennifer B. Gordetsky
Melinda Lerwill
Anna Marie Mulligan

Liron Pantanowitz
David Papke,
Pathologist-in-Training
Carlos Parra-Herran
Rajiv M. Patel
Deepa T. Patil
Charles Matthew Quick
Lynette M. Sholl
Olga K. Weinberg
Maria Westerhoff
Nicholas A. Zoumberos,
Pathologist-in-Training

ABSTRACT REVIEW BOARD

Benjamin Adam
Rouba Ali-Fehmi
Daniela Allende
Ghassan Allo
Isabel Alvarado-Cabrero
Catalina Amador
Tatjana Antic
Roberto Barrios
Rohit Bhargava
Luiz Blanco
Jennifer Boland
Alain Borczuk
Elena Brachtel
Marilyn Bui
Eric Burks
Shelley Caltharp
Wenqing (Wendy) Cao
Barbara Centeno
Joanna Chan
Jennifer Chapman
Yunn-Yi Chen
Hui Chen
Wei Chen
Sarah Chiang
Nicole Cipriani
Beth Clark
Alejandro Contreras
Claudiu Cotta
Jennifer Cotter
Sonika Dahiya
Farbod Darvishian
Jessica Davis
Heather Dawson
Elizabeth Demicco
Katie Dennis
Anand Dighe
Suzanne Dintzis
Michelle Downes

Charles Eberhart
Andrew Evans
Julie Fanburg-Smith
Michael Feely
Dennis Firchau
Gregory Fishbein
Andrew Folpe
Larissa Furtado
Billie Fyfe-Kirschner
Giovanna Giannico
Christopher Giffith
Anthony Gill
Paula Ginter
Tamar Giorgadze
Purva Gopal
Abha Goyal
Rondell Graham
Alejandro Gru
Nilesh Gupta
Mamta Gupta
Gillian Hale
Suntrea Hammer
Malini Harigopal
Douglas Hartman
Kammi Henriksen
John Higgins
Mai Hoang
Aaron Huber
Doina Ivan
Wei Jiang
Vickie Jo
Dan Jones
Kirk Jones
Neerja Kambham
Dipti Karamchandani
Nora Katabi
Darcy Kerr
Francesca Khani

Joseph Khoury
Rebecca King
Veronica Klepeis
Christian Kunder
Steven Lagana
Keith Lai
Michael Lee
Cheng-Han Lee
Madelyn Lew
Faqian Li
Ying Li
Haiyan Liu
Xiuli Liu
Lesley Lomo
Tamara Lotan
Sebastian Lucas
Anthony Magliocco
Kruti Maniar
Brock Martin
Emily Mason
David McClintock
Anne Mills
Richard Mitchell
Neda Moatamed
Sara Monaco
Atis Muehlenbachs
Bitu Naini
Dianna Ng
Tony Ng
Michiya Nishino
Scott Owens
Jacqueline Parai
Avani Pendse
Peter Pytel
Stephen Raab
Stanley Radio
Emad Rakha
Robyn Reed

Michelle Reid
Natasha Rekhman
Jordan Reynolds
Andres Roma
Lisa Rooper
Avi Rosenberg
Esther (Diana) Rossi
Souzan Sanati
Gabriel Sica
Alexa Siddon
Deepika Sirohi
Kalliopi Siziopikou
Maxwell Smith
Adrian Suarez
Sara Szabo
Julie Teruya-Feldstein
Khin Thway
Rashmi Tondon
Jose Torrealba
Gary Tozbikian
Andrew Turk
Evi Vakiani
Christopher VandenBussche
Paul VanderLaan
Hannah Wen
Sara Wobker
Kristy Wolniak
Shaofeng Yan
Huihui Ye
Yunshin Yeh
Anjana Yeldandi
Gloria Young
Lei Zhao
Minghao Zhong
Yaolin Zhou
Hongfa Zhu

To cite abstracts in this publication, please use the following format: **Author A, Author B, Author C, et al. Abstract title (abs#). In "File Title." *Laboratory Investigation* 2021; 101 (suppl 1): page#**

238 Reduced S-100 Expression in Melanoma Assessed by Digital Image Analysis Predicts Poor Overall Survival

Ibrahim Abukhiran¹, Ilham Farhat¹, Andrew Bellizzi¹, Sarag Boukhar¹

¹University of Iowa Hospitals & Clinics, Iowa City, IA

Disclosures: Ibrahim Abukhiran: None; Ilham Farhat: None; Andrew Bellizzi: None; Sarag Boukhar: None

Background: S-100 differential expression is believed to be pathogenetically associated with melanoma development and progression. Furthermore, studies have showed strong correlation between serum S-100-B concentrations and therapy response or tumor progression, with few reports of diminished or lost S-100 antigenicity in metastatic melanoma. SOX10 is also believed to play a critical role in melanoma cell invasion. However, the prognostic value of S-100 and SOX10 immunohistochemical (IHC) expression is not well-studied. Herein, we report digital image analysis (DIA) of S-100 and SOX10 expression in a large cohort of well-annotated melanomas, finding a significant relationship between S-100 expression and overall survival.

Design: S-100 and SOX10 IHC were performed on tissue microarrays (TMAs) from 273 melanoma cases (ascertained between 2010 and 2017) from 248 patients (137 primaries, 136 metastases). BAP1 and BRAF V600E mutation-specific IHC had been previously performed. Glass slides were digitally scanned (3DHISTECH, Budapest, Hungary) and whole TMA cores were annotated. Optimized membranous (S-100) and nuclear (SOX10) 3DHISTECH QuantCenter algorithms were used to count and threshold (1+, 2+, 3+) immunoreactive tumor cells (ITC). A strong positivity index [(SPI) percentage of total strong positive (+3) cells to total positive cells] and weighted positivity index (WPI) were recorded for each stain. The WPI was calculated according to the following formula: $WPI = [(strong\ ITC\% \times 3) + (moderate\ ITC\% \times 2) + (weak\ ITCx1)]/3 \times 100$. The cases were stratified into WPI or SPI high ($\geq 55\%$) and low ($< 55\%$) expressing categories. Survival analysis (K-M curve with Mantel-Cox test), t-test, and one-way ANOVA were used with $p < 0.05$ considered significant.

Results: Survival analysis showed a statistically significant difference ($p = < 0.0001$) in overall survival between the S-100-SPI high ($\geq 55\%$), low ($< 55\%$), and S-100-negative cases. The median survival (in weeks) was 517, 98, and 65 for SPI high, low, and negative cases, respectively. There were also statistically significant differences in S-100 SPI according to histologic type, location, and BAP1 status (Table 1). There was no survival difference between the high and low score groups for SOX10-SPI (0.8798), SOX10-WPI ($p = 0.3689$), or S-100-WPI ($p = 0.9727$).

Association of S100 Strong Positivity Index to Clinicopathologic Variables			
		Average S100 SPI	p
Metastatic		70	0.31
Primary		73	
Cutaneous		73	0.0004
Non-cutaneous		61	
BAP1	Intact	72	0.033
	Lost	60	
BRAF V600E	Negative	71	0.84
	Positive	73	

Figure 1 - 238

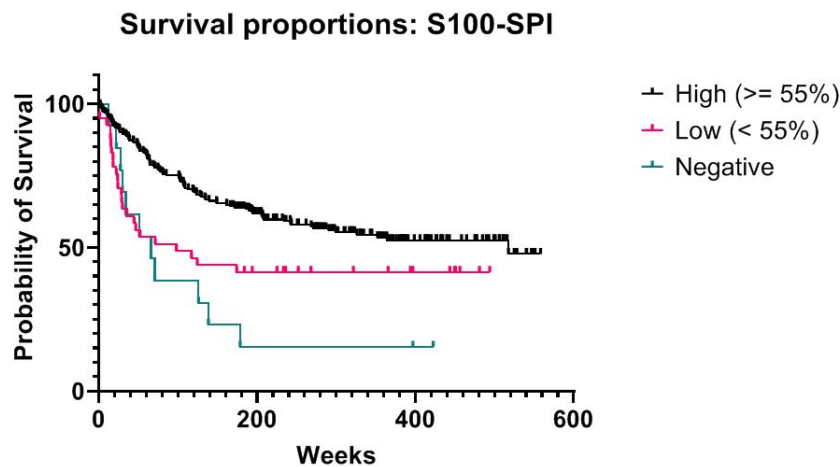


Figure-1: Kaplan-Meier curve showing a statistically significant difference ($p < 0.0001$) in overall survival between cases with high, low and negative S100-SPI score.

Conclusions: High S-100 (but not SOX10) SPI is associated with a significant survival benefit in melanoma. SPI low-status correlated with BAP1 loss and non-cutaneous origin. The S-100 and SOX10 WPI failed to demonstrate prognostic import.

239 Imaging Mass Spectrometry Aids in the Classification of Nevi Versus Melanoma

Rami Al-Rohil¹, Ahmed Alomari², Jason Robbins³, Jessica Moore³, Nathan Patterson⁴, Richard Caprioli⁴, Jeremy Norris⁵

¹Duke University School of Medicine, Durham, NC, ²Indiana University School of Medicine, Indianapolis, IN, ³Nashville, TN, ⁴Vanderbilt University, Nashville, TN, ⁵Vanderbilt University School of Medicine, Nashville, TN

Disclosures: Rami Al-Rohil: None; Jason Robbins: *Advisory Board Member*, Frontier Diagnostics; Jessica Moore: *Employee*, Frontier Diagnostics; Nathan Patterson: *Employee*, Frontier Diagnostics, LLC; Richard Caprioli: None; Jeremy Norris: *Advisory Board Member*, Frontier Diagnostics, LLC

Background: Classification of melanocytic neoplasms relies on histopathologic examination, but multiple studies have shown poor diagnostic reproducibility, even amongst experts. The focus has now shifted to develop tools that objectify the classification to predict the outcomes accurately. Molecular studies have been a useful adjunct; however, they still carry technical and diagnostic limitations. Matrix-Assisted Laser Desorption Ionization Mass Spectrometry (MALDI MS) is a technology with ideal characteristics for in situ molecular analysis. In MALDI profiling experiments, mass spectra are collected from tissues with known pathologic outcomes. These spectra are used to train machine learning classification models. Spectra taken from new tissues can be compared to the models, classified, and scored, providing a classification both on a per spectra and per sample level.

Design: We analyzed various subclasses of unambiguous nevi and melanomas to investigate the validity of imaging mass spectrometry in the classification of melanocytic neoplasms. The rationale behind using unambiguous lesions is to prove the high-performance parameters of such a platform relative to histopathologic evaluation. Three independent board-certified Dermatopathologists were provided deidentified H&E slides of melanocytic neoplasms along with age, sex, and location and were asked to classify the samples as nevi versus melanoma. Spots of interest were annotated by dermatopathologists using a 50 µm spot tool, and the annotated slide image was registered to 6-micron thick serial section for mass spectrometry. Only triconcordant samples were included for training (n=241) and test set (n=92). Twelve cases were deemed challenging which was further classified as favor benign vs favor malignant. Lesions were deemed correctly classified when 85% of the spots agreed with the concordant diagnosis.

Results: The platform detected melanoma with a sensitivity of 97% and a specificity of 100%; per spectra analysis showed a sensitivity of 95.1% and a specificity of 94.8% in the test set. In the challenging lesions: 50% correctly classified, 42% indeterminate, and 8% misclassified.

Conclusions: These findings support the validity of Imaging Mass Spectrometry as an analytical technology in the diagnosis of melanocytic neoplasms and provide an additional layer of evidence to support a consensus diagnosis in challenging lesions while requiring minimal tissue. Further studies to include external validation cohorts of unambiguous and ambiguous tumors are needed to prove clinical utility.

240 Systematic Re-Evaluation of Pathologic Examination and Treatment Modalities in Desmoplastic Melanoma with Emphasis on Advanced Stage

Farah Baban¹, Kabeer Shah², Ruifeng (Ray) Guo¹

¹Mayo Clinic, Rochester, MN, ²St. Mary's Hospital, Madison, WI

Disclosures: Farah Baban: None; Kabeer Shah: None; Ruifeng (Ray) Guo: None

Background: Desmoplastic melanoma (DM) differs from conventional melanoma with distinct morphology and clinical behavior. Management of desmoplastic melanoma has been controversial and variable. Only limited studies have been performed and one of the main challenges is in regard to adjuvant therapy offered in clinically advanced stages.

Design: 75 patients with a diagnosis of DM and a clinical record from our institution were retrospectively evaluated and followed up over a 22 year period from 1998 to 2020. All patients had wide local excision and some of them went on with lymph node examination. The clinical course and treatment modalities of those with metastasis (advanced stage III and IV disease) were reviewed systematically and the findings were summarized.

Results: 20 of 75 patients had metastases either at the time of diagnosis or later in the course of the disease, with 18 of 20 having complete follow up. Among the 18 patients with metastases, only one was limited to the regional draining basin, while all the rest developed distant metastases. The mean age was 67.8 years (range 33-87) with males being predominant 16 versus 4 females. The majority, 13 of 20, received radiation and or conventional chemotherapy after the initial resection to reduce the risk of local recurrence. 7 patients with distant metastases received immune check inhibitors (including Ipilimumab, Pembrolizumab and Nivolumab) treatment. Among them, 5 patients showed complete responses (defined as being clinically and radiographically in remission). The remaining 2 patients that failed to respond had a high disease burden with other comorbidities (metastases to brain and liver). The remaining 11 patients did not receive immune check inhibitors. Among them, 10 of 11 succumbed to the metastatic disease irrespective of any other treatment modalities. The one that survived had an advanced stage III disease treated successfully with tumor resection only.

Conclusions: In our study, DM is characterized by 26.6% metastasis, rarely limited to regional lymph nodes and majority developed distant metastases, which is a distinct feature. In treatment, metastatic DM showed a 71.4 % response rate to immune check inhibitors in our patients in contrast to other modalities, shedding light on encouraging survival outcomes with immunotherapy in this specific melanoma subtype. Larger scale clinical studies are needed.

241 Comprehensive Single-Cell Analysis of Peripheral Blood in Sézary Syndrome Reveals Novel Expression Markers and Shifting Gene Profiles Associated with Treatment

Nick Borchering¹, Nicholas Henderson², Luana Ortolan³, Vincent Liu², Brian Link⁴, Aaron Mangold⁵, Ali Jabbari²

¹Washington University School of Medicine, St. Louis, MO, ²University of Iowa Carver College of Medicine, Iowa City, IA, ³Seattle Children's Hospital, Seattle, WA, ⁴University of Iowa, Iowa City, IA, ⁵Mayo Clinic Arizona, Scottsdale, AZ

Disclosures: Nick Borchering: None; Nicholas Henderson: None; Vincent Liu: None; Aaron Mangold: *Consultant, Kirin; Grant or Research Support, MiRagen; Grant or Research Support, Solagenix; Grant or Research Support, Sun Pharma; Grant or Research Support, Elorac*

Background: Although central to the diagnosis of cutaneous T cell lymphoma (CTCL) is the malignant clonal proliferation of skin-tropic T cells, the term represents a spectrum of diseases often with varied clinical courses. Most patients have an indolent disease course with cycling therapies, while others, especially in advanced stages of disease, have aggressive progression and poor median survival. Adding to the difficulty of treatment, Sézary syndrome (SS), a leukemic variant of CTCL, lacks highly consistent phenotypic and genetic markers that would aid in not only the diagnosis of the malignancy, but also response to therapies.

Design: Using single-cell mRNA and T-cell-receptor sequencing of peripheral blood immune cells in SS, we extensively mapped the transcriptomic variations of nearly 50,000 T cells of both malignant and nonmalignant origins of five patients. The single cells were processed and clustered using R (v4.0.2) with the Seurat R package (v3.2.2) using uniformed manifold approximation approach. TCR sequences were organized using our scRepertoire R package (0.99.17) in order to create measures of clonality that could interact with the seurat object.

Results: We identified potential diverging SS cell populations, including quiescent and proliferative populations shared across multiple patients. In a single patient, we were able to characterize differences in cell populations comparing malignant T cells at the start of histone deacetylase inhibition (HDACi) and photopheresis to a secondary time point after progression on treatment. New cellular clusters after progression on the therapy had increased expression of the transcriptional factor *FOXP3*.

Conclusions: This study is the first cohort of whole-transcriptome single-cell quantification of SS patients in the peripheral blood. Although a clonal tumor, we demonstrate SS at the single-cell mRNA level mirrors the heterogeneity of findings reported in clinical and flow-based investigations. Despite this, the resolution offered by highthroughput single-cell techniques could allow for precision diagnostics, new avenues for applied and basic sciences, and even possible therapeutic monitoring.

242 PD-L1 Expression in HPV-Dependent Versus HPV-Independent Invasive Vulva Squamous Cell Carcinoma

Chau Bui¹, Fabiola Medeiros¹, Brian Cox¹, Mariza De Peralta-Venturina¹, Bonnie Balzer¹

¹Cedars-Sinai Medical Center, Los Angeles, CA

Disclosures: Chau Bui: None; Fabiola Medeiros: None; Brian Cox: None; Mariza De Peralta-Venturina: None; Bonnie Balzer: None

Background: PD-L1 has become increasingly useful to predict response to checkpoint inhibitor therapy in squamous cell carcinomas (SCCs) of various anatomic sites. Approximately 90% of vulvar cancers are SCCs. Two etiological pathways have been implicated in the pathogenesis of vulvar SCC: a high-risk human papillomavirus (HPV)-dependent route associated with p16 positivity and an HPV-independent pathway characterized by TP53 mutations. Some studies suggest that HPV-dependent cancers have a more favorable prognosis. To date, large-scale data on the presence of PD-L1 or other immunotherapy targets in vulvar cancer are lacking. The aim of this study was to assess the association between PD-L1 expression and vulva SCC subtype in order to evaluate the utility of PD-L1 in prognostication and therapeutic selection based on HPV status.

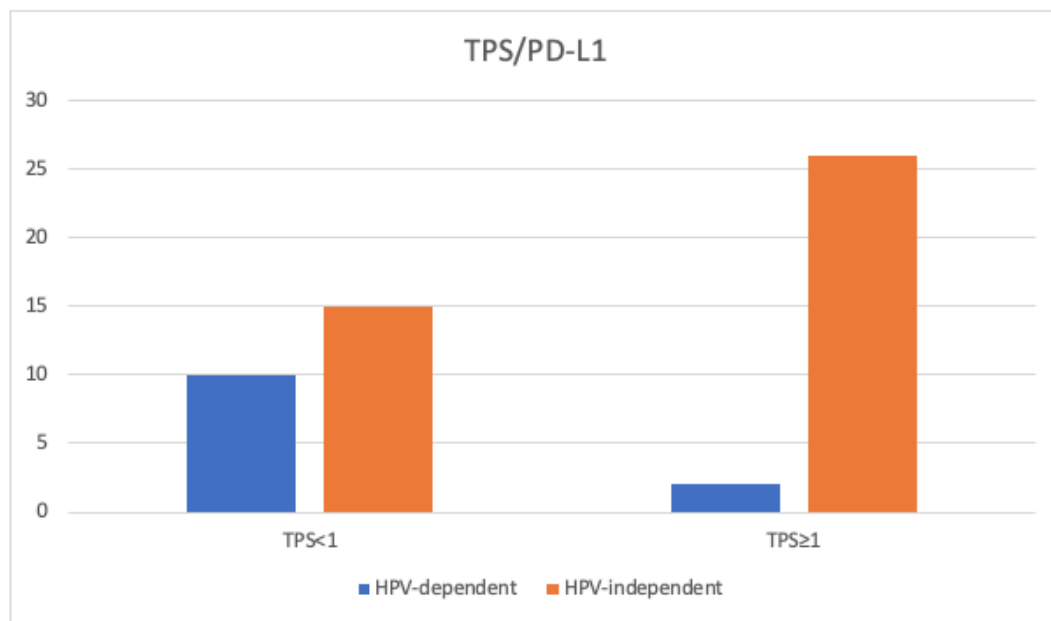
Design: Fifty three biopsy and resection specimens of invasive vulvar SCC were collected from a tertiary medical center over a 15-year span. Staining with H&E, p16, p53, and PD-L1 IHC was performed on cut tissue sections. Expression of P53 was classified as wild-type (scattered or mild-epithelial) or mutant (basal expression, diffuse overexpression, absent, or cytoplasmic). PD-L1 status was assessed using the immune cell score(IC) defined by <1% and >1%; the Tumor proportion score (TPS) defined by <1%, >1%, and >50%; and the Combined positive score (CPS) defined by <1, >1, and >10. The primary outcome was PD-L1 expression as compared between HPV-dependent (block positive p16 and wild-type p53) and HPV-independent (mutant p53 and negative or patchy positive p16) tumors based on chi-square test.

Results: The study group consisted of 25 HPV-dependent and 28 HPV-independent VSCC from patients aged 34 to 91 years. PD-L1 positivity was observed in the majority of cases in both groups (60-96.4%) (Table 1). There was a statistically significant difference between HPV-dependent and HPV-independent tumors based on TPS ($p=0.007$) (Figure 1). However, PD-L1 expression based on IC ($p=0.453$) and CPS ($p=0.176$) showed no significant difference between groups.

Percent	IC<1	IC>1	TPS<1	TPS>1	TPS>50	CPS<1	CPS>1	CPS>10
HPV-dependent	20	80	40	52	8	16	68	16
HPV-independent	10.7	89.3	7.1	57.1	35.7	3.6	50	46.4

Percent of PD-L1 positivity

Figure 1 - 242



Conclusions: This study demonstrates that PD-L1 expression is detectable in a substantial proportion of invasive vulvar SCCs, with a significantly greater association between PD-L1 and HPV-independent tumors as compared with HPV-dependent tumors. These findings suggest that PD-L1 testing is warranted in all PD-L1 vulvar SCC subtypes, although HPV-independent tumors as a whole may be more responsive to PD-L1 inhibitor therapy.

243 Characterization of the Immune Landscape of Acral Lentiginous Melanomas in Caucasian and Hispanic Populations

Woo Cheal Cho¹, Rossana Lazcano Segura¹, Luisa Solis Soto¹, Edwin Parra¹, Sandro Casavilca Zambrano², Miluska Castillo³, Carlos Castaneda², Pavandeep Gill¹, Priya Nagarajan¹, Doina Ivan¹, Jonathan Curry, Ignacio Wistuba¹, Victor Prieto¹, Carlos Torres-Cabala¹, Phyu Aung¹

¹The University of Texas MD Anderson Cancer Center, Houston, TX, ²Instituto Nacional de Enfermedades Neoplásicas, Lima, Peru, ³Lima, Peru,

Disclosures: Woo Cheal Cho: None; Rossana Lazcano Segura: None; Luisa Solis Soto: None; Edwin Parra: None; Sandro Casavilca Zambrano: None; Miluska Castillo: None; Carlos Castaneda: None; Pavandeep Gill: None; Priya Nagarajan: None; Doina Ivan: None; Jonathan Curry: None; Ignacio Wistuba: None; Victor Prieto: None; Carlos Torres-Cabala: None; Phyu Aung: None

Background: Highly immunogenic, cutaneous melanomas (CMs) are frequently associated with tumor-infiltrating lymphocytes (TILs), and the presence of a dense lymphocytic infiltrate correlates with improved response to immune checkpoint inhibitors (ICIs) in patients with CMs. Unlike CMs arising in the non-acral sites, acral lentiginous melanomas (ALMs), the most common melanoma subtype in non-Caucasians, often exhibit a low density of TILs and express PD-L1 less frequently, making them potentially less susceptible to ICIs. It is unknown whether the immune landscape of ALM is associated with ethnicity. This knowledge could contribute to a better prognostication of ALM in specific populations and identify new therapeutic targets.

Design: We performed 7-color multiplex immunofluorescence (mIF) assay, using a panel composed of SOX10, CD3, CD8, CD68, PD-1, PD-L1 and DAPI, in 36 ALMs from two different ethnic groups (18 Caucasians and 18 Hispanics). The immune infiltrates from 5 intratumoral regions of interest were analyzed using a digital image analysis software to determine the cell density of each immune phenotype. IHC testing for IDO-1 and CD20 was also performed on selected cases. Statistical analysis was performed to compare the immune landscape between the two groups with respect to clinicopathologic characteristics.

Results: ALMs in Hispanic patients showed a higher median cell density of cytotoxic T-cells (CD3+/CD8+) ($p=0.03$), antigen-experienced T-cells (CD3+/PD1+) ($p=0.03$) (Figure 1), and antigen-experienced cytotoxic T-cells (CD3+/CD8+/PD1+) ($p=0.02$), when compared with those in Caucasian patients (Table 1 and Figure 2). Overall, a lower clinical stage was associated with a higher density of macrophages expressing PD-L1 ($p=0.04$) (Figure 2).

Phenotypes	Co-localized markers	Hispanics median cell density (n/mm ²)	Range	Caucasians median cell density (n/mm ²)	Range	P-value
T-cell	CD3+	459.8	37.7-2717.3	148.6	29.0-2110.1	
Cytotoxic T-cell	CD3+/CD8+	132.6	5.3-470.0	26.2	3.5-1030.1	0.03
T-cell, antigen-experienced	CD3+/PD1+	65.2	6.6-1842.2	23.3	0-657.2	0.03
Cytotoxic T-cell, antigen-experienced	CD3+/CD8+/PD1+	32.5	1.8-197.3	5.6	0-616.9	0.02
T-cell PD-L1+	CD3+/PD-L1+	76.8	0-326.6	18.4	0-415.6	
Cytotoxic T-cell PD-L1	CD3+/CD8+/PDL1+	58.5	0-271.4	7.7	0-341.3	
T-cell, antigen-experienced, PD-L1+	CD3+/CD8+/PD1+	25.4	0-172.4	6.0	0-284.9	
Cytotoxic T-cell, antigen-experienced, PD-L1+	CD3+/CD8+/PD1+/PD-L1+	18.7	0-150.5	3.3	0-271.9	
Macrophage	CD68+	118.5	2.0-362.9	81.2	23.1-428.9	
Macrophage, PD-L1+	CD68+/PD-L1+	3.9	0-20.4	0.8	0-225.0	
B-cell	CD20+	11.1	0.7-256.5	9.6	1.0-102.0	
IDO-1	IDO-1+	2.7	0-73.5	12.6	0-222.1	

Figure 1 - 243

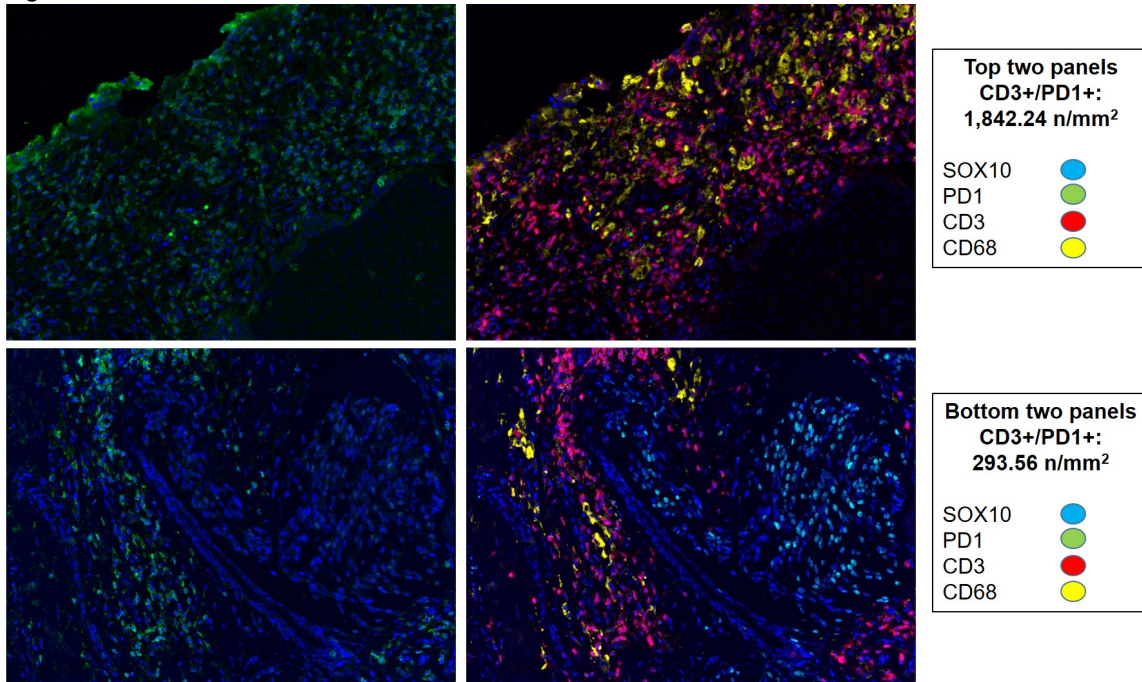


Figure 1. Representative examples of antigen-experienced T-cells (CD3+/PD1+) by mIF.

Figure 2 - 243

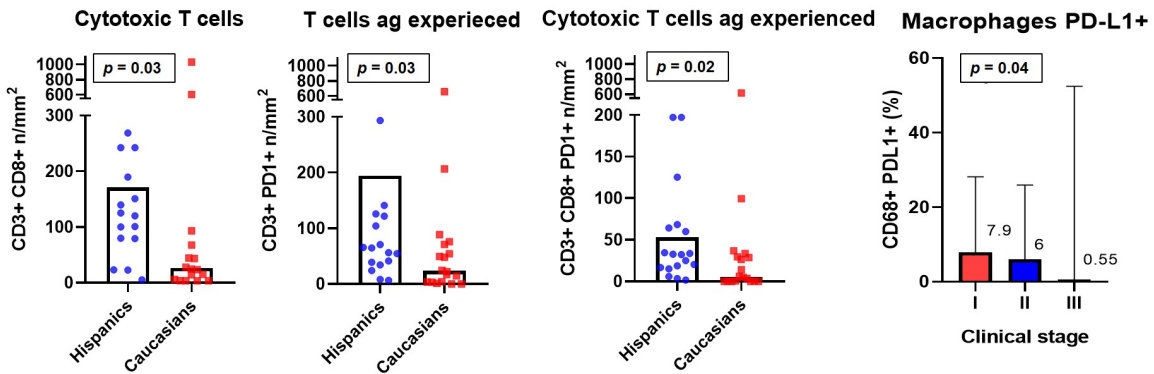


Figure 2. Immune phenotypes showing statistically significant ($p < 0.05$) differences between Caucasian and Hispanic populations (each bar indicates median). Association between clinical stages and percentage of macrophages expressing PD-L1 (each vertical line indicates range).

Conclusions: There was a significant difference in the immune landscape of ALMs between Caucasian and Hispanic patients, particularly with the density of cytotoxic T-cells, antigen-experienced T-cells and antigen-experienced cytotoxic T-cells within the tumor microenvironment, suggesting a role for ethnicity in the response to ICIs. These findings also suggest the importance of individualized prognostic risk stratification for patients of different ethnicities. Further evaluation of survival with regards to the composition, density and distribution of TILs is warranted to assess their prognostic values across different ethnic groups.

244 The Utility of Telomerase Reverse Transcriptase Immunohistochemistry as a Surrogate Marker of TERT Gene Amplification Status in Acral Lentiginous Melanoma

Woo Cheal Cho¹, Wen Li², Jun Gu¹, Wei-Lien (Billy) Wang¹, Jing Ning¹, Steven Sfamenos¹, Pavandeep Gill¹, Priya Nagarajan¹, Jonathan Curry¹, Doina Ivan¹, Alexander Lazar¹, Victor Prieto¹, Carlos Torres-Cabala¹, Phyu Aung¹

¹The University of Texas MD Anderson Cancer Center, Houston, TX, ²McGovern Medical School at UTHealth, The University of Texas Health Science Center at Houston, Houston, TX

Disclosures: Woo Cheal Cho: None; Wen Li: None; Jun Gu: None; Wei-Lien (Billy) Wang: None; Jing Ning: None; Steven Sfamenos: None; Pavandeep Gill: None; Priya Nagarajan: None; Jonathan Curry: None; Doina Ivan: None; Alexander Lazar: None; Victor Prieto: None; Carlos Torres-Cabala: None; Phyu Aung: None

Background: Acral lentiginous melanomas (ALMs) exhibit a high degree of copy number (CN) alterations, often with amplifications of the telomerase reverse transcriptase (*TERT*) gene, which are associated with adverse prognosis. Despite the prognostic value of *TERT* amplification in ALMs, fluorescent in situ hybridization (FISH) for *TERT* is not performed routinely in pathology laboratories. Here, we assess the utility of TERT protein expression by immunohistochemistry (IHC) as a potential surrogate marker of *TERT* amplification in ALMs.

Design: IHC for TERT was performed on a series of 35 acral and nonacral melanomas, including 18 primary and 3 metastatic ALMs. The proportion and intensity of TERT expression were evaluated, and H-score was calculated. FISH was performed, using a probe binding to *TERT* at 5p15 and a normalization probe that hybridizes to 5q31. Fisher’s exact test and Spearman’s correlation were used to evaluate the associations between two categorical and continuous variables, respectively. Logistic regression was used to assess the relationship between binary variables and other predictors. The predictive ability was evaluated by using receiver operating characteristic (ROC) curve and the area under ROC curve (AUC).

Results: The frequency of TERT expression and *TERT* amplification, as well as results of statistical analysis, are summarized in Table 1 and Figure 1. Overall, TERT immunoreactivity was significantly associated with *TERT* amplification in our cohort ($p=0.009$). By logistic regression models, the intensity of TERT expression and H-score were associated with *TERT* amplification ($p=0.03$ and $p=0.047$, respectively). AUCs for the proportion of TERT expression, intensity of TERT expression, and H-score were 0.77, 0.83, and 0.77, respectively. Moderate (2+) intensity of TERT expression correlated with high *TERT* amplification ratio, with a correlation coefficient of 0.37 ($p=0.03$).

		Number (%) of lesions				Overall (n = 35)
		PALM (n = 18)	MALM (n = 3)	PNLAM ^a (n = 8)	PNACM (n = 6)	
TERT protein expression by IHC		11 (61%)	3 (100%)	2 (25%)	3 (50%)	19 (54%)
<i>TERT</i> gene amplification by FISH ^b		4 (22%)	2 (67%)	0 (0%)	1 (17%)	7 (20%)
Overall correlation between TERT protein expression and <i>TERT</i> gene amplification						
		TERT protein expression by IHC			P value 0.009	
		Absent (n = 16)		Present (n = 19)		
<i>TERT</i> gene amplification status, n (%)	Absent	16 (100%)		12 (63%)		
	Present	0 (0%)		7 (37%)		
Overall prediction performance of proportion and intensity of TERT protein expression^c and H-score^d on <i>TERT</i> gene amplification						
		P value in logistic regression model		Area under ROC curve		
Proportion of TERT protein expression		0.05		0.77		
Intensity of TERT protein expression		0.03		0.83		
H-score		0.047		0.77		
Overall correlation of proportion and intensity of TERT protein expression^c and H-score^d with <i>TERT</i> amplification ratio						
		Correlation coefficient		P value		
Proportion of TERT protein expression		0.29		0.10		
Intensity of TERT protein expression		0.37		0.03		
H-score		0.30		0.08		
Abbreviation: PALM, primary acral lentiginous melanoma; MALM, metastatic acral lentiginous melanoma; PNLAM, primary nonlentiginous acral melanoma; PNACM, primary nonacral cutaneous melanoma; TERT, telomerase reverse transcriptase; IHC, immunohistochemistry; FISH, fluorescent in situ hybridization; ROC, receiver operating characteristic						

^a Nonlentiginous acral melanoma represents a rare group of acral melanomas without lentiginous growth pattern, showing features compatible with other histologic subtypes of cutaneous melanomas arising in nonacral sites (e.g., nodular or superficial spreading subtype).

^b *TERT* gene amplifications were considered positive if the ratio between *TERT* gene copy number and control was greater than 1.11, the cutoff value of which was established at our institution through probe validation and statistical analysis.

^c The proportion of melanoma cells expressing TERT (cytoplasmic) was recorded in percentage. The intensity of TERT protein expression was recorded as negative (0), weak (1+), moderate (2+), or strong (3+), using the keratinocytes of stratum spinosum and luminal cells of eccrine glands/ducts as reference intensities (designated as 2+ and 3+ intensities, respectively). H-score was calculated using the formula: [(% of positive cells) × (intensity of protein expression)]

Figure 1 - 244

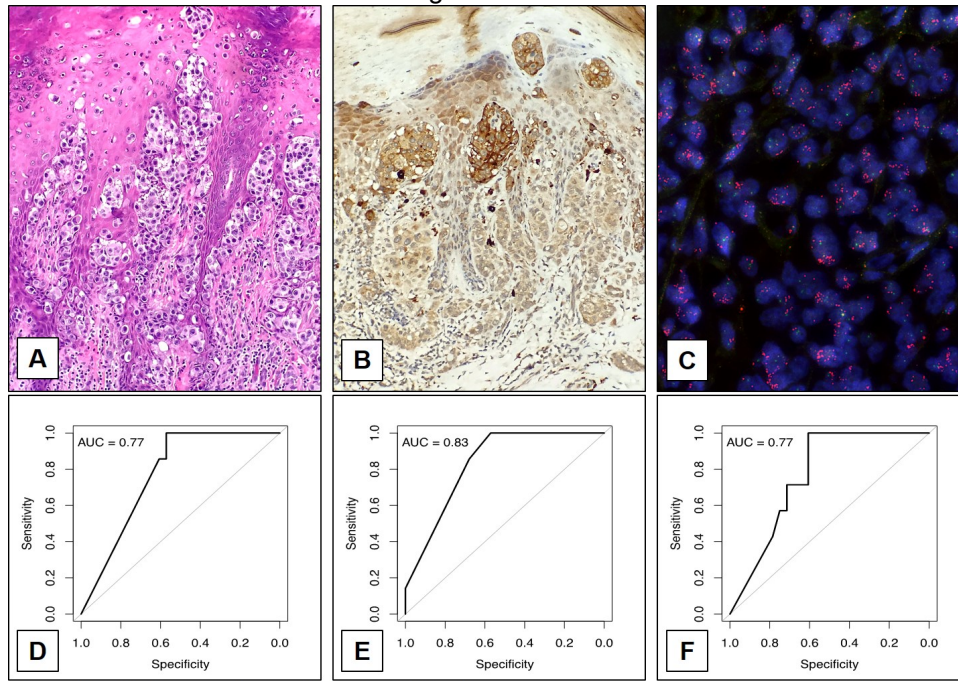


Figure 1. Acral lentiginous melanoma (A) showing TERT protein expression (B) by immunohistochemistry and *TERT* gene amplification by FISH (C). ROC curves for the association between *TERT* gene amplification and proportion of TERT expression (D), intensity of TERT expression (E), and H-score (F).

Conclusions: In our study, TERT protein expression was more common in metastatic ALMs than in primary ALMs, suggesting a role for *TERT* in the progression of ALMs. TERT expression, particularly with intensity of at least moderate (2+), correlated well with *TERT* amplification in our cohort, suggesting potential utility of IHC to predict *TERT* amplification status in ALMs. Additional studies with larger cohorts are needed to further elucidate the value of TERT IHC as a surrogate marker of *TERT* amplification status in ALMs.

245 Molecular Profiling of Syringocystadenocarcinoma Papilliferum Reveals RAS-Activating Mutations and a UV-Signature

Kristine Cornejo¹, Lloyd Hutchinson², Patrick O'Donnell³, Xiuling Meng⁴, Sara Shalin⁵, David Cassarino⁶, May Chan⁷, Timothy Quinn⁸, Paul Googe⁹, Rosalynn Nazarian¹⁰

¹Massachusetts General Hospital, Boston, MA, ²UMass Memorial Health Care, Worcester, MA, ³University of Massachusetts, Worcester, MA, ⁴UMass Medical School, Worcester, MA, ⁵University of Arkansas for Medical Sciences, Little Rock, AR, ⁶Kaiser Permanente Los Angeles, ⁷University of Michigan, Ann Arbor, MI, ⁸Massachusetts General Physicians Organization Dermatopathology Associates, Newton, MA, ⁹University of North Carolina, Chapel Hill, NC, ¹⁰Harvard Medical School, Boston, MA

Disclosures: Kristine Cornejo: None; Lloyd Hutchinson: None; Patrick O'Donnell: None; Xiuling Meng: None; Sara Shalin: None; David Cassarino: None; May Chan: None; Timothy Quinn: None; Paul Googe: None; Rosalynn Nazarian: None

Background: Syringocystadenocarcinoma papilliferum (SCACP) is an exceedingly rare cutaneous adnexal carcinoma and is the malignant counterpart of syringocystadenoma papilliferum (SCAP). SCAP is commonly

located on the head and neck and may arise in association with a nevus sebaceus. *RAS* mutations have been identified in SCAP (*HRAS* in up to 26% of cases) and nevus sebaceus (*HRAS* in up to 95% of cases; *KRAS* in up to 5% of cases), but the molecular profile of SCACP has not been explored. The aim of this study is to review the clinicopathologic features and molecular profile of SCACP.

Design: We obtained a total of 11 SCACP cases from 6 institutions and reviewed the clinical characteristics and morphologic features. In addition, we performed molecular profiling using next generation sequencing by employing the Ampliseq Cancer Hotspot Panel v2 analyzing 50 cancer “hotspot” gene mutations.

Results: The clinicopathologic and mutation profiles are summarized in Figure 1. The cohort comprised of 6 females and 5 males with ages ranging from 29-96 (mean: 73.6) years. The neoplasms occurred on the head and neck (n=8; 73%) and extremities (n=3; 27%), of which one arose in association with a nevus sebaceus on the scalp. Morphologically, 4 cases showed at least carcinoma in situ (adenocarcinoma: n=2; squamous cell carcinoma: n=2) and 7 cases were invasive with variable components of adenocarcinoma and squamous cell carcinoma/carcinoma with squamous differentiation. Eight of 11 (73%) cases identified hotspot mutation(s) consisting of *HRAS* (n=4), *KRAS* (n=1), *TP53* (n=4), *ATM* (n=2), *FLT3* (n=1), *CDKN2A* (n=1) and *PTEN* (n=1). UV-associated mutations defined as C>T or CC>TT at dipyrimidine sites were identified in *TP53*, *CDKN2A* and *ATM*. Two cases were not found to harbor hotspot mutations and 1 case failed due to poor DNA quality/quantity. All 4 cases with *HRAS* mutations occurred on the head and neck, while the case with a *KRAS* mutation occurred on the lower extremity.

Figure 1 - 245

Age	Sex	Location	Tumor	<i>HRAS</i>	<i>KRAS</i>	<i>TP53</i>	<i>FLT3</i>	<i>ATM</i>	<i>CDKN2A</i>	<i>PTEN</i>	
71	M	Scalp	Invasive	■			■				
89	F	Thigh	Invasive		■			■	■		
57	M	Scalp	In situ	■							
93	M	Ear	Invasive	■		■		■			
66	M	Scalp	In situ	■							
89	F	Forearm	Invasive	FAIL							
61	F	Scalp	Invasive								
92	F	Forearm	Invasive			■					
29	F	Scalp	Invasive								
96	M	Ear	In situ			■				■	
64	F	Scalp	In situ			■					

Clinical Characteristics	
Age	
■	0-50 years (n=1)
■	51-80 years (n=5)
■	>80 years (n=5)
Sex	
■	Male (n=5)
■	Female (n=6)
Location	
■	Head & Neck (n=8)
■	Extremity (n=3)
Tumor	
■	In situ (n=4)
■	Invasive (n=7)

Conclusions: *RAS*-activating mutations were detected in 45% of cases, of which the majority (80%) involved *HRAS* and occurred on the head and neck, supporting these tumors are a result of malignant transformation of SCAP and is an early event. Additional UV-associated mutations also occurred in *TP53*, *CDKN2A* and *ATM* in sun-exposed sites. These findings suggest SCACP displays a diversity of oncogenic drivers and the additional tumor suppressor inactivating mutations, which appear to be UV-related, play a role in malignant progression.

246 Ultrasensitive RNAscope In Situ Hybridization is a Cost-Effective Method for Determining Clonality in Cutaneous B-cell Lymphomas and Lymphoproliferative Disorders

Ashley Craddock¹, William Kane², Alejandro A. Gru², Sarah Gradecki²

¹University of Virginia Health System, Charlottesville, VA, ²University of Virginia, Charlottesville, VA

Disclosures: Ashley Craddock: None; William Kane: None; Alejandro A. Gru: *Primary Investigator*, Innate Pharma; Sarah Gradecki: None

Background: Demonstrating clonality is critical in the diagnosis of cutaneous B-cell lymphoma; however, the relatively lower expression levels of kappa and lambda light chains in B-cells as compared to plasma cells limits

reliable detection. Several methods are currently available to assess light chain restriction in formalin-fixed, paraffin-embedded tissue: immunohistochemistry, conventional in situ hybridization (ISH), and ultrasensitive RNAscope in situ hybridization (RNAscope). Often, ISH and PCR studies for IgH heavy chain rearrangements are both performed to increase the likelihood of detecting clonality or to confirm clonality.

Design: Institutional archives were searched for all cases of cutaneous B-cell lymphoma and atypical lymphoid infiltrates diagnosed from 2016 to 2020. Use of ISH, RNAscope, and IgH rearrangement studies was documented. The use of IgH rearrangement studies in ISH vs. RNAscope and equivocal vs. polyclonal vs. restricted groups was compared using Fishers’ exact tests. Additionally, a cost analysis comparing the cost to patient and lab when using ISH vs. RNAscope was performed.

Results: 280 cases were identified, with ISH or RNAscope performed on 186 (66.4%). Conventional ISH was performed on 109 (58.6%) and RNAscope was performed on 77 (41.4%) (Table 1). Significantly fewer IgH rearrangement studies were performed on cases that were evaluated with RNAscope as compared to ISH (p=0.03). Subgroup analysis demonstrated that there was no significant difference in the use of IgH studies in cases that were equivocal (p=0.35) or polyclonal (p=0.76), but cases that were restricted by RNAscope were significantly less likely to have subsequent IgH studies performed (p=0.02). Factoring in the risk of IgH testing as associated IgH costs, the expected cost of cases using ISH was \$1054.03 to the patient and \$245.66 to the lab, while the expected cost using RNAscope was just \$828.00 to the patient and \$229.32 to the lab.

Table 1: Rates of IgH gene rearrangement study use in cutaneous B-cell lymphomas and atypical lymphoid infiltrates with conventional in situ hybridization or RNAscope in situ hybridization

	Conventional ISH (N=109)	RNAscope (N=77)	P value
IgH Rearrangement	27 (24.8%)	9 (11.7%)	0.03
Equivocal	13 (11.9%)	7 (9.1%)	
IgH Rearrangement Performed	5 (38.5%)	1 (14.3%)	0.35
IgH Rearrangement Not Performed	8 (61.5%)	6 (85.7%)	
Polyclonal	29 (26.6%)	24 (31.2%)	
IgH Rearrangement Performed	9 (31.0%)	6 (25.0%)	0.76
IgH Rearrangement Not Performed	20 (69.0%)	18 (75.0%)	
Restricted	67 (61.5%)	46 (59.7%)	
IgH Rearrangement Performed	13 (19.4%)	2 (4.4%)	0.02
IgH Rearrangement Not Performed	54 (80.6%)	44 (95.6%)	

Conclusions: The use of ultrasensitive RNAscope in situ hybridization to evaluate clonality in cutaneous B-cell lymphoma reduced the need for ordering subsequent IgH rearrangement studies when compared to conventional ISH. In particular, cases with clear light chain restriction by RNAscope did not need confirmation by PCR for IgH rearrangement. Despite higher costs to the lab to run RNAscope, routine use of this methodology can result in cost savings to both the patient and lab by decreasing use of expensive molecular methods.

247 Identifying Signature Genes Associated with Cutaneous Melanoma Survival

Negin Farsi¹, James Cotelingam², Ali Mahdavi Adeli³, Ashish Patil², Diana Veillon²

¹LSU Health Shreveport, Shreveport, LA, ²Louisiana State University Health Sciences Center, Shreveport, LA, ³Memphis, TN

Disclosures: Negin Farsi: None; James Cotelingam: None; Ali Mahdavi Adeli: None; Ashish Patil: None; Diana Veillon: None

Background: Cutaneous melanoma (CM) is responsible for less than 5% of all skin cancers but accounts for most skin cancer deaths. The incidence of CM has been increasing over the past decade and ranks second in rate of new cancer cases in 2019. Although staging and management of CM has been established, there has not been reliable germline variants for CM clinical outcome predictors. While several studies have used gene sequencing in CM cases to determine possible gene alterations, it is not clear how gene alterations, individually and collectively, impact patient survival. For example, BRAF mutations are seen in 40-60% of melanoma cases but do not significantly impact patient survival rates. The purpose of this study is to identify which genes are altered in CM cases and which alterations significantly affect survival.

Design: We curated a list of 51,309 human genes using the consensus coding sequence gene list from the Ensembl Genome Browser website. We then used Cbioportal, a multi-institutional web-based platform that curates data on cancer genomics from prior literature as well as The Cancer Genome Atlas database, to check whether alterations in each individual gene are associated with CM and whether such gene alterations have an impact on overall survival. Cbioportal contains 12 main studies on CM including 1635 samples before October 2020, which we queried for each of the 51,309 genes. The type of mutation in genes, overall survival, disease specific survival, disease free survival, and progression free survival of patients with altered and unaltered genes are calculated from the retrieved results.

Results: Out of 51,309 human genes, we identified 26,931 genes that were sequenced in the 1635 samples. We selected genes with highly significant difference in survival between patients with altered and unaltered genes (p-value<10⁻⁷). We identified 12 signature genes that have a significant effect on decreased overall survival. Analysis of these 12 genes showed that disease specific median survival for patients is reduced to 9.07 months (P-value: 4.91e-4, Attributable Risk: 33-45%) with alterations in these genes, whereas the median survival in unaltered cases is 63.35 months (Table 1). Moreover, the overall survival in cases with altered genes was significantly reduced in comparison to unaltered cases (Figure 1).

Identified Genes: SLX1B, SULT1A4, SNORD32A, SNORD33, SNORD34, SNORD35A, TMEM160, RPL13AP5, INAFM1, GNG8, GSK3A, NAPSB			
	Number of cases Total	Number of Cases Deceased	Median months overall
Altered group	33	31	9.07
Unaltered group	1166	598	63.35

Table 1. Number of cases in altered and unaltered groups for the 12 identified signature genes

Figure 1 - 247

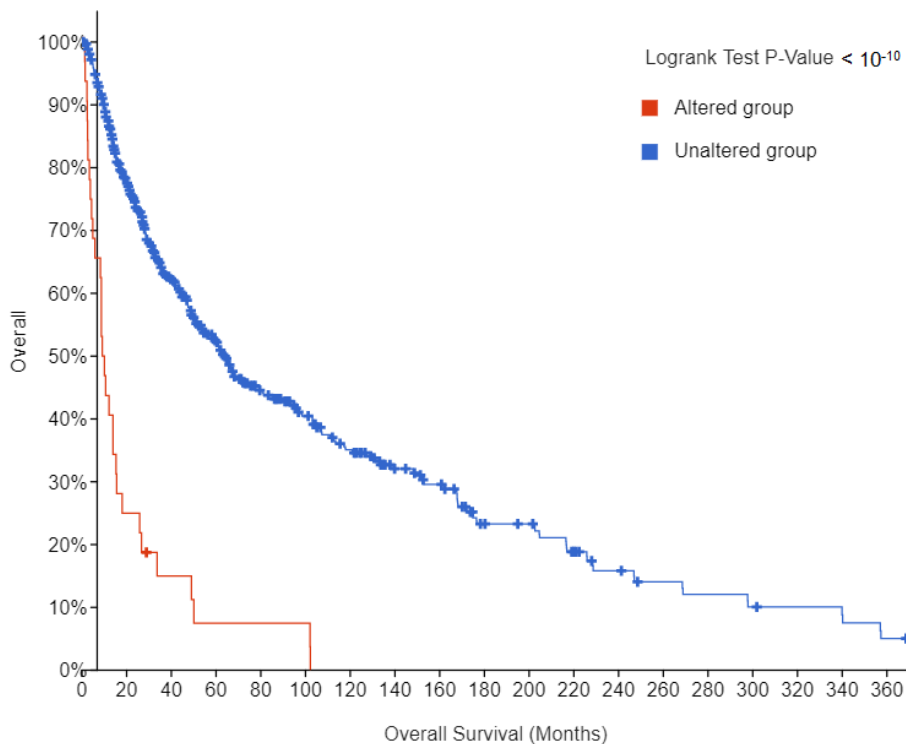


Figure 1. Overall Survival of Altered and Unaltered Groups

Conclusions: The 12 signature genes identified in this study can be used to detect poor prognosis in CM cases and could be viable candidates for future studies and targeted gene therapy.

248 Genomic Copy Number Profiling of Benign and Malignant Cutaneous Melanocytic Neoplasms

Katherine Geiersbach¹, Ruifeng (Ray) Guo¹, William Sukov¹, Thomas Flotte¹, Lori Erickson¹
¹Mayo Clinic, Rochester, MN

Disclosures: Katherine Geiersbach: None; Ruifeng (Ray) Guo: None

Background: Single nucleotide polymorphism (SNP) array profiling with molecular inversion probes can detect genome wide copy number variation (CNV) and loss of heterozygosity (LOH) in DNA samples extracted from formalin fixed, paraffin embedded (FFPE) tissue specimens. Genomic profiling is increasingly employed in the pathologic work up of cutaneous melanocytic neoplasms of indeterminate malignant potential. However, the sensitivity and specificity of SNP array for accurate diagnostic classification of early melanoma is not well characterized, in part due to variable diagnostic thresholds across different pathology practices.

Design: Our study included 30 benign cutaneous nevi and 34 malignant cutaneous melanomas that were diagnosed and clinically followed at our institution. DNA for SNP array testing was extracted from areas on FFPE tissue slides containing at least 40% tumor. All melanomas were confirmed to be malignant by the presence of metastatic disease. Reportable abnormalities on SNP array included technically acceptable calls covering melanoma genes, deletions 1 Mb or larger, duplications 2 Mb or larger, or LOH regions 10 Mb or larger. Known benign or non-pathogenic alterations on SNP array were excluded from analysis.

Results: Benign nevi were mostly normal; only two showed any alterations on SNP array: a 41.5 Mb deletion on 3q in one benign nevus, and a 72.9 Mb deletion on 9q and 22.5 Mb copy gain on 17q in another benign nevus. All melanomas were abnormal with 3 to >100 alterations. Common CNV alterations in melanoma included regions

targeted by a clinically available FISH panel, including gain of 6p, loss of 6q, loss of 9p, gain of 8q, and gain of 11q; however, 5 out of 34 (14.7%) melanomas were negative for abnormalities detected by the FISH panel. In our study, limited to neoplasms that were clearly benign or clearly malignant, the presence of at least one reportable abnormality on SNP array was 100% sensitive and 93% specific for melanoma. Using a threshold of >3 abnormalities, SNP array was 97% sensitive and 100% specific for melanoma.

Conclusions: Genomic copy number profiling is a valuable ancillary test method for detecting genomic abnormalities associated with melanoma. In clinical practice, the sensitivity and specificity of SNP array can be affected by the individual laboratory's handling and reporting of SNP arrays as well as the threshold for establishing a histopathologic diagnosis of melanoma.

249 Squamoid Eccrine Ductal Carcinoma: A Clinicopathologic and Transcriptomic Profiling

Pavandeep Gill¹, Elizabeth Keiser¹, Jiexin Zhang¹, J. Jack Lee¹, Dzifa Duose¹, Baili Zhang¹, Woo Cheal Cho¹, Phyu Aung¹, Michael Tetzlaff², Carlos Torres-Cabala¹, Jonathan Curry¹, Victor Prieto¹, Doina Ivan¹, Priya Nagarajan¹

¹The University of Texas MD Anderson Cancer Center, Houston, TX, ²University of California San Francisco, San Francisco, CA

Disclosures: Pavandeep Gill: None; Elizabeth Keiser: None; Jiexin Zhang: None; J. Jack Lee: None; Dzifa Duose: None; Baili Zhang: None; Woo Cheal Cho: None; Phyu Aung: None; Michael Tetzlaff: None; Carlos Torres-Cabala: None; Jonathan Curry: None; Victor Prieto: None; Doina Ivan: None; Priya Nagarajan: None

Background: Squamoid eccrine ductal carcinoma (SEDC) is a recently described, rare cutaneous neoplasm with a biphasic pattern of growth with squamous and eccrine ductal differentiation. Although little is known about its histogenesis and molecular profile, it is typically associated with an aggressive clinical course. Here, we utilized a novel gene expression profiling platform to characterize the transcriptomic landscape of SEDC, as compared to squamous cell carcinoma (SCC) and eccrine porocarcinoma (EP). To our knowledge, this is the first study to employ this novel molecular diagnostic assay based on quantitative nuclease protection and next-generation sequencing in the evaluation of cutaneous neoplasms.

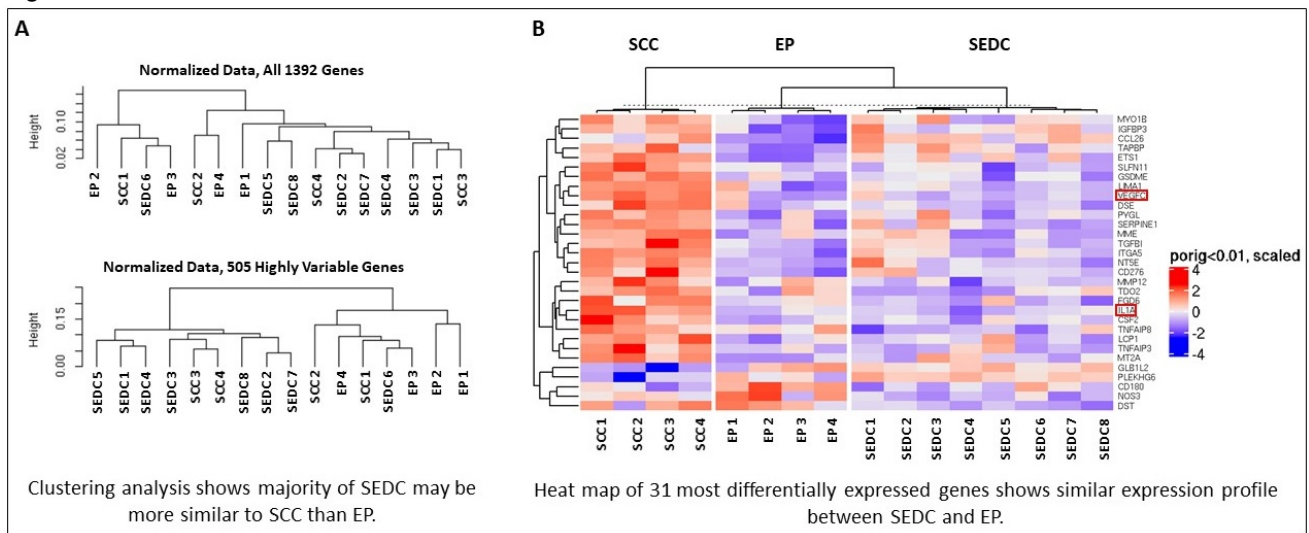
Design: We identified 8 SEDC, 4 SCC, and 4 EP cases from pathology archives to comprehensively collate the clinicopathological and outcome parameters (**Table 1**) and utilize the novel immuno-oncology panel to evaluate gene expression profiles on unstained slides cut from formalin-fixed, paraffin embedded tissues. Pearson correlation and ward.D2 linkage rule were used for clustering analysis, while ANOVA was used to identify differentially expressed genes (DEG).

Results: Cox proportional hazards model revealed a significant univariate association between ulceration and time to recurrence (109.4 months sooner on average, $p < 0.006$) and lymphovascular invasion and regional metastases ($p = 0.01$) in SEDC. A clustering analysis of all 1392 and 505 highly variable genes showed that most SEDC ($n=7$, 87.5%) were more similar to SCC than EP; but the distance between the branches was not significant as evident from the small height (**Figure 1A**). However, SEDC and EP notably under-expressed a majority of 31 DEGs compared to overexpression in SCC via ANOVA analysis (**Figure 1B**), with *IL1A* and *VEGFC* transcript levels most differentially expressed (BH adjusted p -value < 0.05). Among SEDC tumors, the following clinical and gene associations were identified: lymphovascular invasion: *HELLS*, *DTL*, *BORA*, *GSDME*, *GINS4*, and *C20orf24*; metastases: *MME*; angiotropism: *EPCAM*, and tumor size: *IL1RL1* and *ITGA6*; but did not reach statistical significance due to limited sample size.

Table 1: Clinicopathologic features of the squamoid eccrine ductal carcinoma (SEDC), squamous cell carcinoma (SCC), and eccrine porocarcinoma (EP).

Parameter		SEDC, n=8	SCC, n=4	EP, n=4
Mean age (years)		76	80.5	66.5
Sex	Female	2	0	2
	Male	6	4	2
Anatomic site	Head and neck	6	3	1
	Trunk	0	1	1
	Extremities	2	0	2
Epidermal connection	Absent	2	0	0
	Present	6	4	4
Ulceration	Absent	5	1	2
	Present	3	3	2
Level of Invasion	Dermis	2	0	1
	Subcutis	6	4	3
Histologic grade	G1	0	0	1
	G2	5	1	2
	G3	3	3	1
Perineural invasion	Absent	1	0	3
	Present	7	4	1
Angiotropism	Absent	4	2	3
	Present	4	2	1
Lymphovascular invasion	Absent	6	3	3
	Present	2	1	1
Any Metastasis	Absent	4	2	3
	Present	4	2	1
Regional metastasis	Absent	4	2	3
	Present	4	2	1
Distant metastasis	Absent	7	2	3
	Present	1	2	1
Outcome	Dead	1	2	0
	Alive	7	2	3
	Lost to follow up	0	0	1

Figure 1 - 249



Conclusions: Our study shows that SEDC shares gene expression profiles with both SCC and EP, ulceration and lymphovascular invasion may correlate with SEDC tumor recurrence and regional metastases, respectively, and certain genes may correlate with clinical progression. Additional studies using larger cohorts are necessary to validate these findings.

250 Characterizing the Molecular Landscape of Acral Lentiginous Melanoma: A Multi-National Study of 429 Patients

Pavandeep Gill¹, Kenjiro Namikawa², Denai Milton¹, Woo Cheal Cho¹, Priya Nagarajan¹, Doina Ivan¹, Jonathan Curry¹, Victor Prieto¹, Carlos Torres-Cabala¹, Phyu Aung¹

¹The University of Texas MD Anderson Cancer Center, Houston, TX, ²National Cancer Center Hospital, Tokyo, Japan

Disclosures: Pavandeep Gill: None; Kenjiro Namikawa: *Speaker*, Ono Pharmaceutical; *Speaker*, Bristol Myers Squibb; *Speaker*, Novartis Pharma; *Speaker*, MSD; Denai Milton: None; Woo Cheal Cho: None; Priya Nagarajan: None; Doina Ivan: None; Jonathan Curry: None; Victor Prieto: None; Carlos Torres-Cabala: None; Phyu Aung: None

Background: Acral lentiginous melanoma (ALM) is a rare, distinct subtype of cutaneous melanoma. It is typically associated with a delayed diagnosis and worse prognosis than other cutaneous melanoma subtypes. It also constitutes a relatively greater proportion of melanomas occurring in non-Caucasians. Risk factors for ALM remain unclear and the genetic alterations associated with ALM remain to be further defined. We performed a multi-national study, including the largest cohort of ALM patients reported to date, in order to better characterize the molecular landscape of this disease.

Design: We identified 429 patients with ALM who underwent mutational testing at two major cancer referral centers in the United States (US, n=376) and Japan (n=53) between 2000 and 2020. Platforms for mutational testing included next generation sequencing and polymerase chain reaction panels. We collected clinico-pathological, outcome, and molecular data for all patients. The frequency of mutations was calculated, and a Fisher exact test was used to compare the rates of *BRAF*, *KIT*, *NRAS*, *HRAS*, and *KRAS* mutations between the US and Japanese populations.

Results: Molecular alterations were identified in 316 of the 429 (74%) patients. The overall frequencies of *BRAF*, *KIT*, *NRAS*, *HRAS*, and *KRAS* were 29%, 27%, 28%, 3%, and 2%, respectively. Significant differences between the frequency of *HRAS* mutations in the Japanese and US populations were observed (8% and 2% respectively, p <0.05). No other significant differences were identified. Ninety of the 316 (28%) cases included other mutations involving *TP53*, *GNAQ*, *TERT*, *PTEN*, *NF1*, *CTNNB1*, *MET*, *CBL*, *CDKN2A*, and *APC* genes.

Conclusions: In the largest reported study of the mutational landscape of ALM, we confirm that *BRAF*, *KIT*, and *NRAS* mutations are the most commonly identified genetic alterations comprising 84% of all mutations identified in ALM. Molecular alterations were not identified in 26% of patients, suggesting that other genetic and/or epigenetic events may be involved. Our study enhances our knowledge of the genetic landscape of ALM and offers insights into potential therapeutic targets.

251 Merkel Cell Polyomavirus–Negative Merkel Cell Carcinoma is Associated with JAK-STAT and MEK-ERK Pathway Activation

Takeshi Iwasaki¹, Michiko Matsushita², Kazuhiko Hayashi³, Daisuke Nonaka⁴, Kenichi Kohashi⁵, Yuichi Yamada⁶, Satoshi Kuwamoto⁷, Yoshihisa Umekita², Yoshinao Oda⁵

¹JCHO Kyushu Hospital, Kitakyushu, Japan, ²Tottori University, Japan, ³Tottori University Medicine, ⁴Guy's and St. Thomas' Hospital NHS Foundation Trust, United Kingdom, ⁵Kyushu University, Fukuoka, Japan, ⁶Kyushu University, Japan, ⁷Tottori University, Yonago, Japan

Disclosures: Takeshi Iwasaki: None; Michiko Matsushita: None; Kenichi Kohashi: None; Yuichi Yamada: None; Yoshinao Oda: None

Background: Merkel cell polyomavirus (MCPyV) is monoclonally integrated into the genomes of approximately 80% of Merkel cell carcinomas (MCCs). It affects clinicopathological features of MCC, and MCPyV large T-antigen (MCPyV-LT) has a pivotal role in MCC pathogenesis. However, the molecular mechanisms involved in MCC development after MCPyV infection are unclear. The association between MCPyV infection and the MEK-ERK and JAK-STAT signaling pathway activation in MCC was investigated to elucidate the molecular pathogenesis of MCC with regard to signal transduction. The aim was to identify new molecular targets for MCC treatment.

Design: The molecular pathological characteristics of 30 MCPyV-positive and 20 MCPyV-negative MCC were analyzed; MCPyV was detected through real-time polymerase chain reaction. Using next-generation sequencing, mutations of oncogenes in eight cases (MCPyV-positive in four cases, MCPyV-negative in four cases) were found. Further, immunohistochemical expression of phosphorylation status of MEK, ERK, JAK, and STAT3. Then, using an in vitro system of MCC cell lines, the activation status of the MEK-ERK and JAK-STAT pathways, as well as the effect of JAK inhibitor was analyzed.

Results: Mutation analysis revealed variants of 21 genes, including 5 pathogenic mutations. JAK2 and JAK3 mutations were not observed. Principal component analysis revealed that MCPyV-positive and MCPyV-negative MCCs are distinguished by the first and second principal components. Immunohistochemically, the expression of pJAK2 ($p = 0.038$) and pERK1/2 ($p = 0.019$) was higher in MCPyV-negative MCCs than in MCPyV-positive MCCs. Conversely, STAT3 phosphorylation status in MCPyV-positive MCCs did not differ from that in MCPyV-negative MCCs. Prognostic analysis revealed that male gender, older age, non-MCPyV status, and advanced cancer stage are unfavorable prognostic factors; however, the phosphorylation statuses of JAK2, STAT3, MEK1/2, and ERK1/2 were not related to the prognosis. In vitro analysis showed that JAK inhibitors inhibited cell proliferation more in MCPyV-negative MCC cell lines (MCC13 and MCC14/2) than in a MCPyV-positive MCC cell line (MKL-1). Western blotting showed that the expression of pERK1/2 and pMEK was higher in MCPyV-negative MCC cell lines than in MCPyV-positive MCC cell lines.

Conclusions: These results suggest that MCPyV-positive and MCPyV-negative MCCs have different tumorigenic pathways and that JAK-STAT and MEK-ERK signaling pathway signals are novel targets for MCC treatment.

252 Cutaneous Apocrine Carcinoma of the Scrotum: A Multi-institutional Clinicopathologic Analysis of 6 Cases and Comparison with Extramammary Paget Disease

Sonia Kamanda¹, Adeboye O. Osunkoya², Jonathan Epstein³, Andres Matoso³

¹James Buchanan Brady Urological Institutions, Johns Hopkins Hospital, Johns Hopkins Medical Institutions, Baltimore, MD, ²Emory University, Atlanta, GA, ³Johns Hopkins Medical Institutions, Baltimore, MD

Disclosures: Sonia Kamanda: None; Adeboye O. Osunkoya: None; Jonathan Epstein: None; Andres Matoso: None

Background: Primary cutaneous apocrine carcinoma (AC) of the scrotum is extremely rare with only 4 case reports published in the literature.

Design: A retrospective multi-institutional review of the pathology and expert consultation files between 1989 and 2020 identified 6 cases of AC of the scrotum. We compared the findings to our recently published series of extramammary Paget disease (EMPD) of the scrotum.

Results: Mean age at presentation was 71 years (range: 31-91 years). Presenting clinical symptoms included an eczematous rash, scrotal cyst, ulcerated skin, and inguinal mass. The tumor ranged in size from 1.2 to 5.5cm. Microscopically, the tumors show a solid growth pattern with involvement of the dermis and hypodermis and are composed of infiltrating cohesive cords and nests of epithelioid cells surrounded by desmoplastic stromal reaction. The cells have an eosinophilic cytoplasm, display nuclear pleomorphism, irregular nuclear membranes, and prominent nucleoli. Glandular/tubule formation and intracellular mucin were seen in 2 cases (33.3%). Focal squamous differentiation was evident in one case (16.6%). An intraductal component was seen in one case (16.6%). Pagetoid spread of tumor cells in the epidermis was seen in 1 case (16.6%). By immunohistochemistry, the tumor cells were most consistently positive for GCDFP15 (4/4), GATA3 (4/4), mammaglobin (2/2), AR (3/3), and CK7 (4/4). Other positive markers include ER (2/3), and Her2 (1/3). Treatment included wide local excision (n=4) and inguinal lymph node dissection (n=1). Adjuvant therapy included chemotherapy (gemcitabine, carboplatin; n=4), herceptin and lupron (n=1) tamoxifen/arimidex (n=1); and radiotherapy (n=1). At the time of this study, three patients (50%) were reported dead of disease, less than 2 years from the time of diagnosis. Four (66.6%) patients developed metastasis to the inguinal and retroperitoneal lymph nodes, liver, bones, and lungs. Three patients had significant lower extremity edema. Molecular analysis on two cases detected a Her2 mutation in one and microsatellite instability in the other. EMPD and AC share the same immunophenotype, suggesting origin from the

same cell type. While EMPD has an insidious presentation and is most commonly an in-situ disease, AC presents as a mass, is deeply invasive, and has an aggressive clinical behavior.

Conclusions: Distinction of AC from EMPD is important for prognostication and management. Similarities with mammary carcinoma raises consideration for breast cancer specific therapy.

253 Malignant Melanoma in Immunocompromised Patients: a Statistical and Pathologic Analysis.

Trevor Killeen¹, Ryan Shanley¹, Vidhyalakshmi Ramesh¹, Alessio Giubellino¹

¹University of Minnesota, Minneapolis, MN

Disclosures: Trevor Killeen: None; Ryan Shanley: None; Vidhyalakshmi Ramesh: None; Alessio Giubellino: None

Background: Malignant melanoma is the leading cause of death from cutaneous malignancies worldwide. Immunocompromised patients have an increased risk of developing cutaneous malignancies, including malignant melanoma. After identifying immunocompromised patients who subsequently developed melanoma, we collected their clinical and histopathologic data to further analyze this relationship.

Design: We manually reviewed our clinical and pathology databases from 2011 to 2019 to identify all immunocompromised patients who subsequently developed melanoma. Death data, when applicable, was obtained from the death database. In total, 97 patients with a combined 117 unique melanoma lesions were identified. Relevant demographic and diagnostic data, as well as available histopathologic data, were recorded.

Results: The most common causes of immunosuppression, in order of frequency, were transplantation; hematologic neoplasms; and HIV/AIDS. Solid organ transplant, specifically kidney transplant, was the most common transplantation subcategory. Superficial spreading melanoma and lentigo maligna melanoma were the most represented subtypes of malignant melanoma. Median Breslow depth was 0.8 mm. The most common primary tumor stage was T1a. A significant portion of patients developed melanoma *in situ* following immunosuppression, instead of or in addition to malignant melanoma. Median time from onset of immunosuppression to melanoma diagnosis was 5 years, with 6 years for all transplants (n=54), 7 years for solid organ transplants (n=41), and 4.5 years for all hematologic neoplasms (n=36). 32 of 97 patients (33%) were deceased at the time of analysis; 6 of these patients (19%) had melanoma listed as a cause of death. Notably, 66 of the total 97 patients (68%) were male.

Conclusions: Our data contribute to an improved understanding of melanoma in immunocompromised patients and the histopathologic profile of melanoma. Transplants, particularly solid organ transplants, are a major contributor to immunosuppression in this patient demographic. Median time between immunosuppression onset and diagnosis of melanoma in our cohort varied based on the cause of immunosuppression, with solid organ transplants showing a higher median disease-free state after onset of immunosuppression than hematologic neoplasms. Further statistical analyses will compare this patient cohort to the general population to establish incidence and hazard ratios for development of melanoma in immunocompromised patients.

254 Different Oncogenic Mechanism Between Caucasians and African Americans for Post-Transplant Skin Cancer

Takeda Kotaro¹, Aisha Kousar¹, Kimbely Briley¹, Lorita Rebellato¹

¹East Carolina University, Greenville, NC

Disclosures: Takeda Kotaro: None; Aisha Kousar: None; Kimbely Briley: None; Lorita Rebellato: None

Background: Transplant medicine is continuously expanding. Increased occurrence of malignancy becomes one of the medical burdens in organ transplant recipients. Skin cancer is the most common malignancy after transplantation. Since different ethnicities have a different cancer risk, different oncogenic mechanism is speculated for skin cancer.

Design: We compared post-renal transplant skin cancer between Caucasians and African Americans. Adult primary renal transplants performed at our transplant center between 2009 and 2015 were included in this study. Skin cancer incidence through 2019 was determined through detailed medical record review. The study evaluated time interval until initial skin cancer diagnosis, affected location, histologic subtype, clinical stage, human papillomavirus infection, treatments, prognosis, immunosuppressive regimen and human leukocyte antigen (HLA) mismatch.

Results: 447 kidney transplant recipients were analyzed (Caucasians 130, African Americans 317). 31 recipients (6.9 %) developed post-transplant skin cancer (Caucasians 24, African Americans 11) with average age of 61 years at diagnosis. The average time interval until cancer diagnosis was 1356 days. Caucasians were significantly more susceptible to skin cancer than African Americans. Skin cancer in Caucasians was developed exclusively on sun-exposed areas such as face, neck and forearm with an evidence of solar elastosis. In contrast, African Americans developed cancer predominantly on genital areas including perianal area and vulva. 75 % of genital skin cancers showed diffuse p16 positivity, indicating human papillomavirus involvement for carcinogenesis. The most common histologic subtype was squamous cell carcinoma (22), followed by basal cell carcinoma (2), whereas no histologic diagnosis was available in 7 cases. Malignant melanoma was not observed. Most cases of skin cancer were either in situ or focally invasive lesions treated by local excision, but two cases showed advanced stages and one African American died due to perianal cancer. No difference in immunosuppression and number of HLA mismatch was found between the races.

Conclusions: We found high incidence of post-transplant skin cancer with different oncogenic mechanism between Caucasians and African Americans. Sun exposure is the important risk factor in Caucasians, whereas human papillomavirus infection/reactivation is involved for African Americans. This study suggests that skin cancer risk stratification based on race after kidney transplantation is warranted.

255 Complete and Heterogeneous Loss of H3K27 Trimethylation Expression in Secondary and Sporadic Angiosarcomas

Andrea Krajisnik¹, Wonwoo Shon¹

¹Cedars-Sinai Medical Center, Los Angeles, CA

Disclosures: Andrea Krajisnik: None; Wonwoo Shon: None

Background: H3K27 trimethylation (H3K27me3) is a well-known epigenetic regulator that is associated with transcriptional repression. H3K27me3 immunohistochemistry has been considered by many authors to be a reliable diagnostic marker for malignant peripheral nerve sheath tumor, although some disagree. Two recent studies have also explored the status of H3K27me3 protein expression in post-irradiation angiosarcomas (AS), yet inconsistent results were reported. In this study, we analyzed a series of well-characterized secondary and sporadic AS for H3K27me3 protein expression.

Design: Cases of AS (39 total cases; 14 post-irradiation/chronic lymphedema, 13 primary cutaneous, and 12 deep soft tissue/visceral) and 10 post-irradiation atypical vascular lesions were retrieved and follow-up was obtained. Representative hematoxylin and eosin-stained slides were re-reviewed to confirm diagnoses. All sections were then stained with H3K27me3 (C36B11, 1:200, Cell Signaling Technology). The percentage of positive tumor cells was semiquantitatively scored (complete loss: <5%, partial loss: 5-75%, and intact >75%). After the initial review, we also developed a dual-color H3K27me3 (nuclear brown) and CD31 (cytoplasmic red) immunohistochemistry and applied it in selected cases of angiosarcoma and atypical vascular lesion.

Results: 19 of 27 (70%) cutaneous AS showed loss of H3K27me3 expression, including 12 of 14 (86%; complete loss 9 and partial loss 3) secondary AS and 7 of 13 (54%; complete loss 5 and partial loss 2) primary AS. We also detected loss of H3K27me3 expression in 9 of 12 (75%; complete loss 7 and partial loss 2) deep soft tissue/visceral AS. All cases of atypical vascular lesions revealed intact H3K27me3 staining. In those selected cases, dual staining for CD31 and H3K27me3 together expedited visualization and allowed for easier assessment of the tumor foci in question.

Conclusions: There may be some diagnostic role for H3K27me3 immunohistochemistry in the distinction of secondary AS from selected potential mimics, such as atypical vascular lesion. Although it shows low sensitivity in

sporadic AS, detection of H3K27me3 loss may also aid in predicting sensitivity to epigenetic-based therapies. Finally, our H3K27me3/CD31 dual-color stain provides more convenient microscopic evaluation and improved accuracy of H3K27me3 status by precisely delineating the neoplastic endothelial cells.

256 Immunohistochemistry for PRAME in the Differential Diagnosis of Melanocytic Lesions of the Nail Apparatus

Andrea Krajisnik¹, Nima Gharavi¹, Mark Faries¹, Matthew Martelli², Wonwoo Shon¹

¹Cedars-Sinai Medical Center, Los Angeles, CA, ²Rush Foundation Hospital, Meridian, MS

Disclosures: Andrea Krajisnik: None; Nima Gharavi: None; Mark Faries: *Advisory Board Member, Novartis; Advisory Board Member, Merck; Advisory Board Member, Array Bioscience; Advisory Board Member, Pulse Bioscience; Advisory Board Member, Bristol Myers Squibb*; Matthew Martelli: None; Wonwoo Shon: None

Background: Nail unit melanocytic lesions present a unique set of diagnostic challenge owing to the unfamiliarity with clinical assessment and the lack of experience with histologic examination. Because the first surgical specimen received in the pathology laboratory is typically a small, sometimes suboptimal biopsy, the distinction between melanoma and its histologic mimics can be difficult. For this reason, there has been continued interest in the development of ancillary markers that may assist in the differential diagnosis of nail unit melanocytic lesions. Up-regulation of PRAME has been reported to be a common event in melanomas, and relatively recently, immunohistochemistry for PRAME has been shown to be helpful in evaluating various melanocytic neoplasms. In this study, we evaluated PRAME protein expression in a series of nail unit melanocytic lesions.

Design: Formalin-fixed, paraffin-embedded sections from 23 nail unit melanomas (including small biopsy and amputation specimens) and 30 control cases including lentigo (13), conventional melanocytic nevus (8), melanocytic activation/hypermelanosis (5), melanocytic nevus/proliferation with "atypia" (3), and junctional Spitz nevus (1) were retrieved. An automated immunohistochemistry system (Ventana BenchMark XT, Ventana Medical systems, Inc., Tucson, AZ) was used for the detection of PRAME, using a commercially available antibody (E711B; Cell Signaling Technology, Danvers, MA). Nuclear staining was scored as negative (<5%), 1+ (5%-25%), 2+ (26%-50%), or 3+ (>51%). Intensity of staining was scored as weak, moderate, or strong.

Results: All melanoma cases were positive for PRAME (3+ in 19, 2+ in 2, and 1+ in 2 cases; strong in 15, moderate in 6, and weak in 2 cases); of note, two weakly positive cases were sections from significantly decalcified amputation specimen. In specimens where the neoplastic cells are limited in number, the staining was restricted to the tumor cells, corresponding to the initial H&E impression. All control cases were completely negative for PRAME expression.

Conclusions: PRAME expression is helpful in distinguishing between melanomas and other nail unit melanocytic lesions. This antibody also proved to be diagnostic valuable in detecting melanoma cells in small biopsy specimens and minimal residual disease. Future larger studies will have to determine the diagnostic value of PRAME expression in borderline nail unit melanocytic lesions.

257 Exploratory Transcriptomic Analyses of Tumor and Microenvironment Signatures in Aggressive Digital Papillary Adenocarcinoma

Zongshan Lai¹, George Jour², Doina Ivan¹, Carlos Torres-Cabala¹, Priya Nagarajan¹, Baili Zhang¹, Dzifa Duose¹, Jonathan Curry¹, Victor Prieto¹, Phyu Aung¹

¹The University of Texas MD Anderson Cancer Center, Houston, TX, ²New York University, New York, NY

Disclosures: Zongshan Lai: None; George Jour: None; Doina Ivan: None; Carlos Torres-Cabala: None; Priya Nagarajan: None; Baili Zhang: None; Dzifa Duose: None; Jonathan Curry: None; Victor Prieto: None; Phyu Aung: None

Background: Aggressive digital papillary adenocarcinoma (ADPA) is a rare but aggressive cutaneous malignant sweat gland neoplasm that occurs in acral skin. Rates of local recurrence and distant metastasis are approximately 35% and 14%, respectively. No histophenotypic parameters can be used to definitely differentiate ADPA from

histologically similar benign adnexal tumors such as hidradenoma, especially in small biopsies. Complete excision or digit amputation is the treatment of choice for localized ADPA and there is no standard treatment for metastatic disease. We used targeted transcriptomics to characterize the tumor microenvironment of ADPA to identify specific gene expression signatures that could potentially serve for identifying immunotherapy and targeted regimens for ADPA as compared to hidradenoma.

Design: We identified 10 ADPA and 10 hidradenomas from the pathology archives and collated the clinicopathological and outcome parameters (Table 1). We conducted RNA analysis using PanCancer IO 360 assay including 770 genes from 24 different immune cell types and 48 gene derived signatures measuring biological variables crucial to the tumor-immune interaction including cell proliferation, angiogenesis and immune inhibitory mechanisms. Statistical analysis was performed using the N-Solver package ($P < 0.01$, $FDR < 0.01$).

Results: Semi-supervised signature-based analysis revealed upregulated B7-H3, Endothelial cells, and TGF-beta signatures in ADPA compared to benign tumors (signature scores of 5.4 vs. 4.5, 5.4 vs. 4.4, and 5.1 vs. 3.9, respectively; p -value < 0.05 ; Fig.1). *KDR* was downregulated in the benign group compared to ADPA ($\log_2FC = -1.14$, $P < 0.0001$, $FDR = 0.06$; Fig.2A). No differences in the tumor inflammation score and the loss signatures in the *JAK-STAT* pathway were noted between the groups. Both groups showed microsatellite-stable transcriptomic signatures. However, a hypermutated signature was seen almost exclusively in ADPA (2 vs 10/12; Fig.2B).

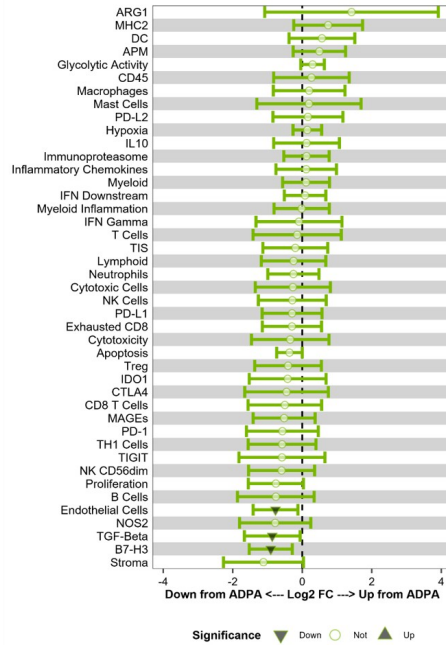
Table1: Patients' demographic and clinicopathological characteristics

Parameters		ADPA (n=9)	Hidradenoma (n=10)
Mean age, years (SD)		47.1 (11.3)	58.6 (14.9)
Sex, n (%)	Female	4 (44.4)	5 (50.0)
	Male	5 (55.6)	5 (50.0)
Race, n (%)	White	8 (88.9)	9 (90.0)
	Black	0 (0)	1 (10.0)
	Unknown	1 (11.1)	0 (0)
Perineural invasion, n (%)	Absent	9 (100.0)	10 (100.0)
	Present	0 (0)	0 (0)
Lymphovascular invasion, n (%)	Absent	7 (77.8)	10 (100.0)
	Present	2 (22.2)	0 (0)
Any Metastasis, n (%)	Absent	7 (77.8)	10 (100.0)
	Present	2 (22.2)	0 (0)
Regional metastasis, n (%)	Absent	8 (88.9)	10 (100.0)
	Present	1 (11.1)	0 (0)
Distant metastasis, n (%)	Absent	7 (77.8)	10 (100.0)
	Present	2 (22.2)	0 (0)
Outcome, n (%)	Dead	1 (11.1)	0 (0)
	Alive	8 (88.9)	10 (100.0)

Note: one of the ADPA cases has two specimens: one from original biopsy and the other one from recurrent lesion)

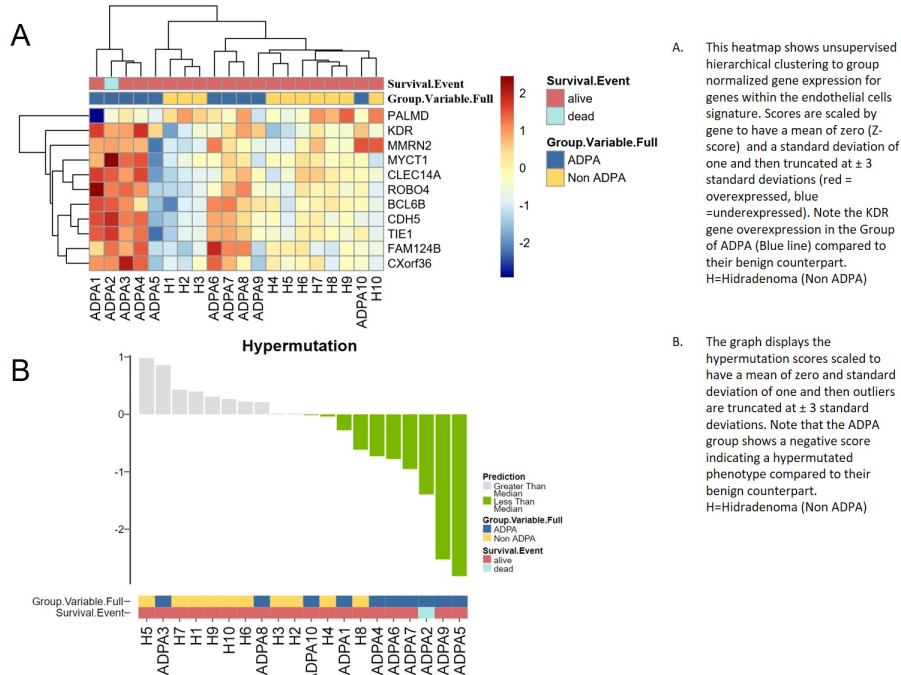
Figure 1 - 257

Results for Group Variable, Hidradenoma vs. ADPA (baseline)



The forest plot shows the differential expression means and 95% confidence intervals between response variables, for each signature. The vertical axis is shown at fold change equal to zero, indicating equivalent expression between the groups. As the marker shifts from the center line there is an increase (shift to the right), or decrease (shift to the left), in the differential expression of that signature when compared to the baseline group ADPA (represented as the vertical line at zero). The shape of the marker (triangle vs circle) in each box indicates whether there is a significant difference in the signature as assessed by univariate analysis. A signature is considered significant if the 95% confidence interval (the horizontal line of the signature) does not cross the vertical axis representing the baseline group and therefore no difference to that baseline group. Not that in the benign group endothelial , TGFB and B7-H3 signature are all downregulated compared to ADPA.

Figure 2 - 257



A. This heatmap shows unsupervised hierarchical clustering to group normalized gene expression for genes within the endothelial cells signature. Scores are scaled by gene to have a mean of zero (Z-score) and a standard deviation of one and then truncated at ± 3 standard deviations (red = overexpressed, blue = underexpressed). Note the KDR gene overexpression in the Group of ADPA (Blue line) compared to their benign counterpart. H=Hidradenoma (Non ADPA)

B. The graph displays the hypermutation scores scaled to have a mean of zero and standard deviation of one and then outliers are truncated at ± 3 standard deviations. Note that the ADPA group shows a negative score indicating a hypermutated phenotype compared to their benign counterpart. H=Hidradenoma (Non ADPA)

Conclusions: Our preliminary result suggests that ADPA lacks a significant tumor inflammatory signature, and lacks microsatellite instability (MSI), which would not support the rationale for using immune checkpoint therapy. The hypermutated signature appears to be specific to ADPA and is independent of the MSI status. *KDR* upregulation in ADPA could serve as a potential target for drugs targeting VEGFR2 which are currently being investigated in clinical trials.

258 Deep Dermal and Subcutaneous Anisometric Cell Lipoma (Dysplastic Lipoma): A Series of Eight Cases

Maryam Masouminia¹, Wonwoo Shon¹

¹Cedars-Sinai Medical Center, Los Angeles, CA

Disclosures: Maryam Masouminia: None; Wonwoo Shon: None

Background: Anisometric cell lipoma, also known as dysplastic lipoma, commonly affects the posterior neck, shoulder, and upper trunk with a male predominance. Striking variation in size and shape of adipocytes can lead to diagnostic confusion, including atypical lipomatous tumor/well-differentiated liposarcoma as one consideration. To the best of our knowledge, there have been no reports in the dermatology or dermatopathology literature describing this peculiar variant of lipoma. In this study, we present a series of eight cases of deep dermal and subcutaneous anisometric cell lipoma.

Design: Eight cases of anisometric cell lipoma were retrieved from our institutional archives. Immunohistochemical stains were performed in all cases included: RB1, p53, and MDM2. Molecular evaluation for MDM2 gene amplification was also performed using FISH on interphase nuclei present on FFPE sections. One selected case was further analyzed by genomic microarray hybridization (OncoScan). Clinical information, including follow-up information, was obtained from our institutional medical record system.

Results: The tumors arose in seven men and one woman, ranging from 29 to 76 years of age (median: 56 years). The sites involved were back (4), shoulder (2), and head and neck (1), and upper arm (1). The tumors ranged from 4 to 14 cm in the greatest dimension (median 8 cm). Microscopically, all tumors were composed of adipocytes with significant variation in size and shape (Fig.1-A) accompanied by minimal cytologic atypia and Lochkern change (Fig1-B). There were also microscopic foci of mild fat necrosis (Fig1-C). Enlarged hyperchromatic stromal cells and thickened fibrous septa, as seen in atypical lipomatous tumor/well-differentiated liposarcoma, were absent. Immunohistochemistry revealed a loss of RB1 nuclear staining in the adipocytic cell nuclei (Fig.2-A). Occasional lesional cells were also positive for p53 protein (Fig.2-B). One case showed some lesional adipocytes with MDM2 protein expression. No MDM2 gene amplification was detected by fluorescence in situ hybridization in all cases (Fig.2-C). By genomic microarray hybridization, the tumor showed a loss of 1q, 7q, 13q, and 16q in one case. At this point, no evidence of recurrent disease or malignant transformation was noted after complete surgical resection.

Figure 1 - 258

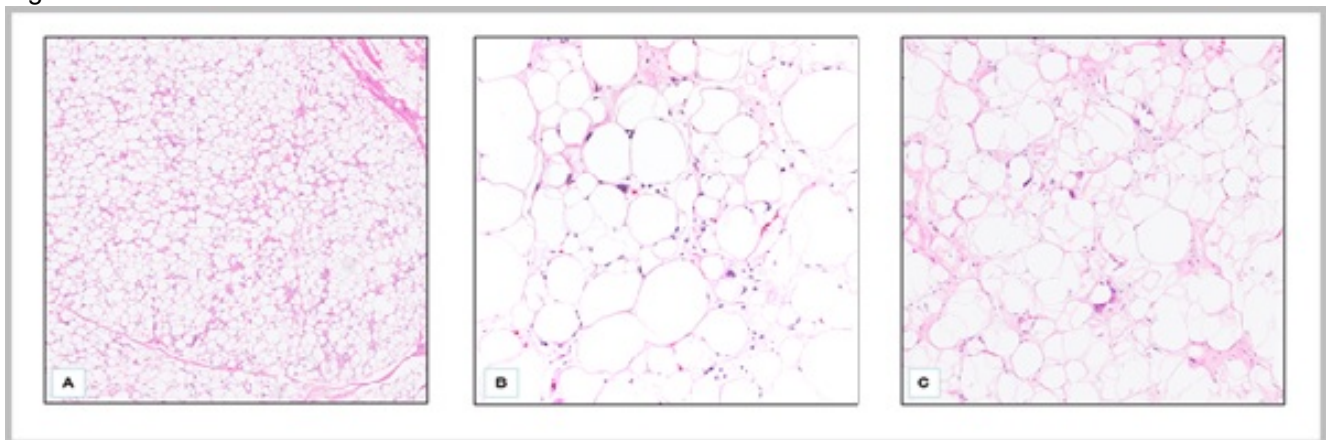
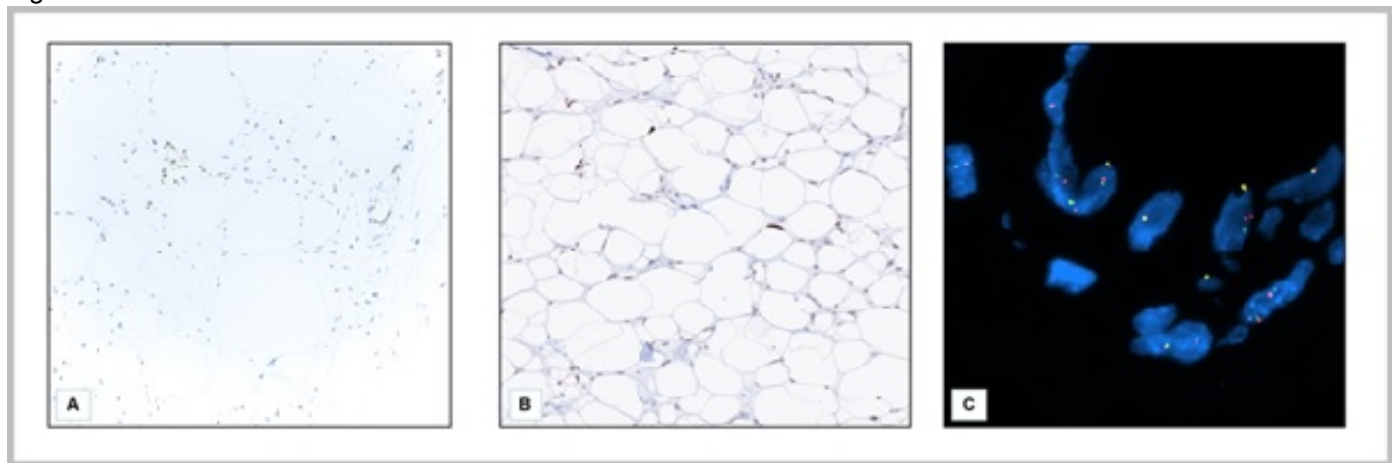


Figure 2 - 258



Conclusions: Anisometric cell lipoma is a rare adipocytic tumor that exhibits distinct histopathologic, immunohistochemical, and genetic features. This underrecognized diagnosis constitutes a diagnostic pitfall for dermatopathologists and dermatologists, and could be misdiagnosed as other benign or malignant lipomatous lesions.

259 Retrospective Clinicopathological Analysis of Clinically Suspicious Cases of Hansen’s Disease

Priyathersini Nagarajan¹, Leena Dennis Joseph¹, Kaviya Bharathi Murugan¹, Priya Nagarajan²

¹Sri Ramachandra Institute of Higher Education and Research, Chennai, India, ²The University of Texas MD Anderson Cancer Center, Houston, TX

Disclosures: Priyathersini Nagarajan: None; Leena Dennis Joseph: None; Kaviya Bharathi Murugan: None; Priya Nagarajan: None

Background: Hansen’s disease caused by *Mycobacterium leprae* is a prevalent infectious disease among the Indian population with high treatment costs. The long incubation period, the wide variability in clinicopathological presentation poses a diagnostic and therapeutic challenge, precluding eradication of the disease. This is further complicated by non-adherence to the prolonged therapy, leading to unusual histologic features. Thus, there is a critical need to re-evaluate the histopathologic features in this context. In this study, we have retrospectively analyzed biopsies from patients who were clinically suspected to have Hansen’s disease in a tertiary care center in south India, over a period of one year from January to December 2019.

Design: We identified 50 skin biopsies from patients with clinically suspected Hansen’s disease from the pathology archives and comprehensively collated the clinical and histopathological information.

Results: The cohort included 36 men and 14 women with a median age of 47.5 years (range 15-80 years) at the time of biopsy. The demographic and clinical information are presented in **Table 1**. The most common clinical presentation was multiple hypopigmented patches with loss of sensation involving face and upper extremities. The duration of symptoms ranged from 1 month to 2 years with an average period of 6 months in most cases. Microscopically 26 cases were confirmed to be Hansen’s disease with lepromatous type (LL) being the most common type (n=11), which showed abundant dermal histiocytic infiltrate with foamy cytoplasm, followed by borderline tuberculoid (n=9), which showed granulomatous dermal infiltrate with perineural predilection, lacking foamy cytoplasm. Of these, 2 cases were from patients with relapse at 8 to 10 years after initial diagnosis and treatment. The modified acid-fast Wade-Fite stain was performed on all biopsies, with positivity in only 3 cases, suggesting low sensitivity, even among LL cases. The most common histopathologic diagnosis among those that were non-diagnostic for Hansen’s disease was polymorphous light eruption with superficial perivascular lymphocytic infiltrate.

Figure 1 - 259

Table 1. Clinical features of patients suspected to have Hansen’s disease

Parameter		n
Median age (years)		47.5
Sex	Female	14
	Male	36
Number of Lesions	Single	11
	Multiple	39
Color of lesions	Hypopigmented	29
	Erythematous	9
Nature of lesions	Patches	20
	Plaques	18
	Papules	2
Sites	Upper limb	11
	Lower limb	7
	Upper & lower limbs	9
	Face	16
	Chest & Back	8
Nerve involvement	Face, extremities & trunk	2
	Ulnar nerve	11
	Radial cutaneous nerve	4
	Great auricular nerve	1
Loss of sensation	Common peroneal nerve	2
	Auriculo-temporal nerve	1
	Median nerve	1
	Decreased	22
	Intact	28
Hair loss	Present	6
	Absent	44

Conclusions: This retrospective study provides a glimpse of the varied clinical and histomorphological features of Hansen’s disease. While the histologic features are most helpful, the utility of ancillary studies is questionable due to low sensitivity of modified acid fast special stains.

260 Experiences With Convolutional Neural Network / Artificial Intelligence Algorithms in the Classification of Pigmented Skin Lesions: Potential Adjunct to Clinical and Histopathologic Assessment

Janira Navarro Sanchez¹, Christopher Lum¹, Shane Spencer², John Shepherd², Kevin Cassel², Mark Willingham²

¹University of Hawaii, John A. Burns School of Medicine, Honolulu, HI, ²University of Hawaii, Honolulu, HI

Disclosures: Janira Navarro Sanchez: None; Christopher Lum: None; Shane Spencer: None; John Shepherd: None; Kevin Cassel: None; Mark Willingham: None

Background: Each year in the US there are more skin cancer diagnoses than all other cancers combined. A significant subset of melanocytic lesions can be diagnostically challenging. In this study we looked at the performance of a Convolutional Neural Network (CNN) in skin lesion classification as a complementary tool to clinical and histologic assessment.

Design: A Neural Network-based classification model was trained on 13842 dermoscopic pictures of histopathology-confirmed pigmented skin lesions from the International Skin Imaging Collaboration (ISIC) Archive dataset. Benign and malignant cases represented 90.7% and 9.2% respectively of the total. The optimal CNN model was selected based on train/validation loss plot, Monte Carlo simulations and receiver operating characteristic curve (AUC/ROC). We performed a blind study of our CNN model with 3 dermatologists on a

comparison batch of 50 images representing benign and malignant skin lesions. Our main outcome measure was accuracy based on AUC/ROC characteristics.

Results: The AUC/ROC of the selected model was 0.948 in the two classification tasks examined: Benign versus Malignant and Melanoma versus Non-Melanoma. The dermatologists and the Artificial Intelligence (AI) comparative image testing showed similar results differentiating benign vs. malignant lesions. Dermatologist 1 and 2 had 70% correct diagnoses, dermatologist 3 had 54% and our CNN model had 68%. There were no incorrectly diagnosed images by the dermatologists and the AI combined.

Conclusions: Artificial intelligence algorithms are a promising tool that can assist dermatologists with melanoma detection in clinical practice. AI scoring of skin pigmented lesions, may provide an objective categorization between low and high risk lesions. This can be useful as an adjunct to histopathological observation of diagnostically challenging lesions, improving the diagnostic accuracy.

261 Weakly-Supervised Deep Learning-Based Segmentation of Non-Melanoma Skin Cancer on Histopathological Images

Trung Nguyen¹, Yufei Zhou¹, Cheng Lu¹, Andrew Janowczyk¹, Rainer Grobholz², Ian Katz³, Anant Madabhushi¹

¹Case Western Reserve University, Cleveland, OH, ²Institute of Pathology, Cantonal Hospital Aarau, Aarau, Switzerland, ³Southern Sun Pathology, Westmead, Australia

Disclosures: Trung Nguyen: None; Yufei Zhou: None; Cheng Lu: None; Andrew Janowczyk: None; Rainer Grobholz: None; Ian Katz: None; Anant Madabhushi: *Advisory Board Member, Aiforia Inc; Grant or Research Support, Bristol Myers-Squibb; Primary Investigator, Astrazeneca; Primary Investigator, Boehringer-Ingelheim*

Background: Non-melanoma skin cancers (NMSC) have a curative rate of > 95% if detected and treated early. A deep learning-based segmentation pipeline may potentially reduce the time needed by pathologists for diagnosing NMSC, but training of such a segmentation approach typically requires a large number of laborious pixel-level tumor annotations. In this study, we present a weakly-supervised segmentation approach using the U-Net (Ronneberger et al., 2015) and CAMEL framework (Xu et al., 2019) that **uses only image-level labels** to automatically delineate regions of Squamous Cell Carcinoma (SCC) and Basal Cell Carcinoma (BCC) on H&E stained histopathological image, obviating the need of pixel-level annotations.

Design: We obtained from 87 patients a collection of 114 digitized H&E stained WSIs at 20x magnification, comprising 10 benign cases, 56 BCC, 10 in-Situ SCC, and 11 invasive-SCC. 550 Region of Interests (ROIs) identified by pathologists were extracted from the WSIs and categorized into 2 classes: 60 non-cancerous (NC) and 490 cancerous (CA) ROIs (i.e. 373 BCC, 53 invasive-SCC, and 64 in-Situ SCC images). These ROIs were randomly split into training and testing sets (ratio of 1:1).

As illustrated in Figure 1, all ROIs are first annotated with image-level labels. Notably, these labels are easy to create yet noisy because CA images contain NC regions as well. An automated Label Refinement procedure was adapted from CAMEL to re-label NC subregions and highlight CA subregions within ROIs labeled as CA. A U-Net model for NMSC tumor segmentation was then trained using the refined labels. A U-Net model using image-level labels as annotations without any label refinement was developed as a comparative strategy (baseline). Our model and the baseline were evaluated against ground truth annotations for CA and NC regions provided by dermatopathologists.

Results: Qualitative results for our model and the comparative approach are illustrated in Figure 2. Compared to the baseline (i.e. U-Net without Label Refinement), our weakly-supervised U-Net model achieved better performance with an F1-score=0.72 and 80.4% accuracy, as opposed to 0.63 and 68.9% for the baseline.

Figure 1 - 261

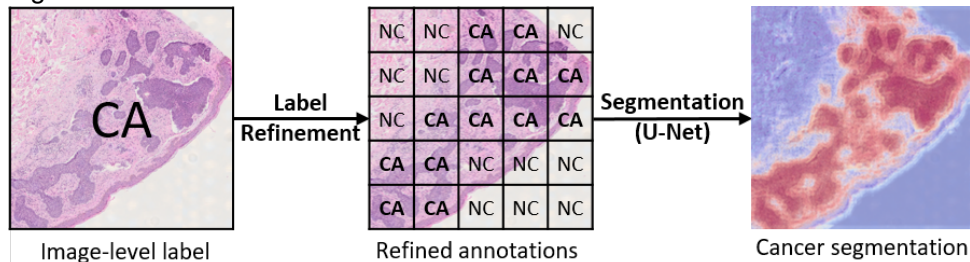


Figure-1. Our pipeline on a CA image. Initially the ROI's annotation is marked with its image-level label (e.g. CA). The Label Refinement procedure provides more granular localization of NC and CA regions within the ROI labeled as CA. The updated labels are fed to U-Net for model training.

Figure 2 - 261

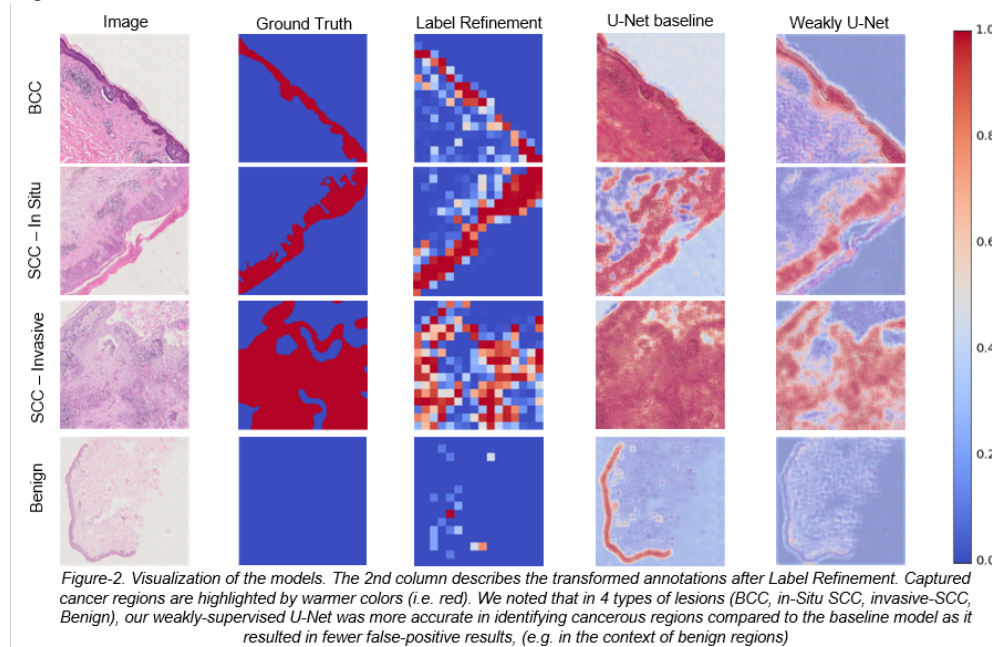


Figure-2. Visualization of the models. The 2nd column describes the transformed annotations after Label Refinement. Captured cancer regions are highlighted by warmer colors (i.e. red). We noted that in 4 types of lesions (BCC, in-Situ SCC, invasive-SCC, Benign), our weakly-supervised U-Net was more accurate in identifying cancerous regions compared to the baseline model as it resulted in fewer false-positive results, (e.g. in the context of benign regions)

Conclusions: These preliminary results suggest that our weakly-supervised U-Net is capable of identifying regions of BCC and SCC. The use of an automated machine learning model for identifying regions of disease on WSIs could help reduce the time for pathologist slide interpretation in rendering a cancer diagnosis.

262 Can Immunohistochemistry On Routine Formalin-Fixed, Paraffin-Embedded Skin Tissue Be Helpful In The Diagnosis Of Bullous Pemphigoid?

Harim Oh, Youngjin Kang¹, Yoo Jin Lee¹
¹Korea University Anam Hospital, Seoul, South Korea

Disclosures: Harim Oh: None; Youngjin Kang: None; Yoo Jin Lee: None

Background: The gold standard for the diagnosis of bullous pemphigoid (BP) is the detection of linear deposition of IgG and/or C3 on the dermoepidermal junction by direct immunofluorescence (DIF). As DIF has several disadvantages because of use of frozen specimens, we hypothesized that immunohistochemical (IHC) staining of complements and IgG using FFPE tissue could help diagnose BP, thereby making immunopathologic confirmation of the bullous process possible without disadvantages of DIF.

Design: Eighty-eight cases of bullous lesions were included. IHC studies for C3d, C4d, and IgG were performed in 88 cases (DIF-confirmed BP [n=43], clinicopathologically suspicious BP with negative DIF results [n=9], and other bullous disease [n=36]). Considering the existence of false-negative DIF results, we compared DIF and IHC staining findings, including those of clinicopathologically suspected BP cases with negative results on DIF.

Results: When the diagnosis was based on C3d, C4d, or IgG positivity on IHC staining, 86% of BP cases diagnosed via DIF could be diagnosed using IHC staining with deposition of C3d, C4d, or IgG as the diagnostic criterium. The sensitivity of IHC staining in detecting BP and suspicious BP cases was similar to that of DIF (80.8% vs. 84.3%), and the specificity was higher (83.3% vs. 75.0%). Furthermore, five of nine (55.6%) cases with negative DIF results could be diagnosed as BP using IHC staining. Considering that DIF is more sensitive than IHC staining, we reviewed IHC-positive and DIF-negative cases and found that 66.7% of discordant cases based on IgG, 100% of discordant cases based on C3d, and 100% of discordant cases based on C4 were treated as BP cases.

Table. Diagnostic value of IHC and DIF based on DIF-confirmed group and highly suspicious group

	Sensitivity		Specificity		PPV		NPV	
	DIF (%)	IHC (%)	DIF (%)	IHC (%)	DIF (%)	IHC (%)	DIF (%)	IHC (%)
IgG	60.8	63.5	94.4	83.3	93.9	84.6	63.0	61.2
C3(d)	76.5	44.2	75.0	100	81.3	100	69.2	55.4
C4(d)	19.6	55.8	100	100	100	100	46.8	61.0
IgG and/or C3(d)	84.3	73.1	75.0	83.3	82.7	86.4	77.1	68.2
C3(d) and/or C4(d)	76.5	61.5	75.0	100	81.3	100	69.2	64.3
IgG and/or C4(d)	62.7	76.9	94.4	83.3	94.1	87.0	64.2	71.4
IgG and/or C3(d) and/or C4(d)	84.3	80.8	75.0	83.3	82.7	87.5	77.1	75.0

BP=bullous pemphigoid, IHC=immunohistochemical, DIF=direct immunofluorescence, PPV=positive predictive value, NPV=negative predictive value

Figure 1 - 262

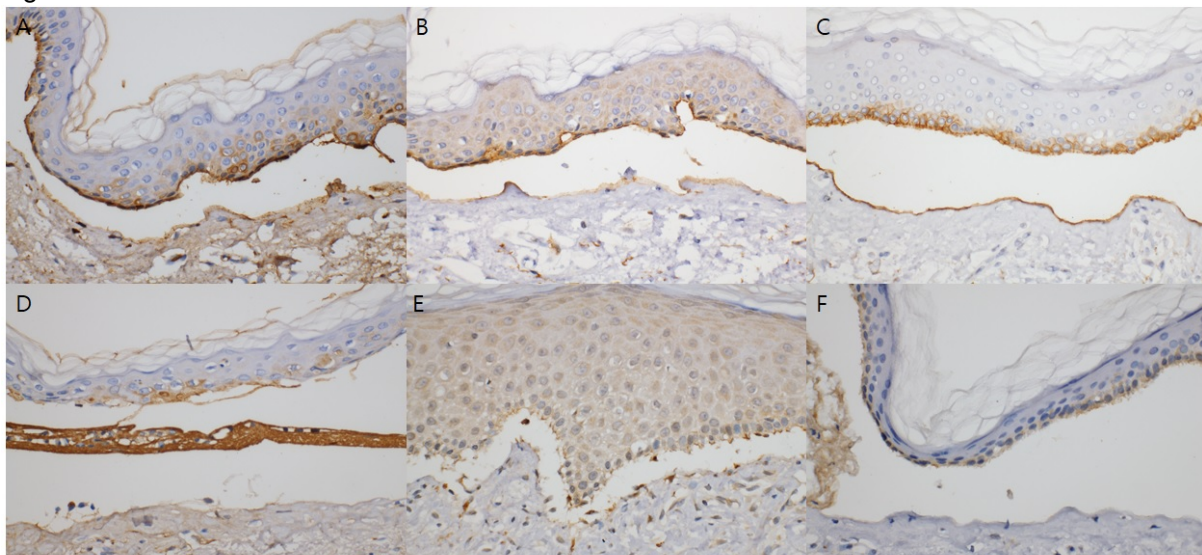


Figure 1. Immunohistochemical staining for IgG, C3d and C4d on formalin-fixed paraffin-embedded tissue:
A to C. Linear deposition of (A) IgG, (B) C3d, (C) C4d along the dermoepidermal junction
D to F. Negative staining of (D) IgG, (E) C3d, (F) C4d (all cases x400)

Conclusions: To the best of our knowledge, our study, which evaluated the diagnostic value of IHC staining as an alternative to DIF, has the second largest number of BP cases yet reported. Although DIF remains the gold standard, IHC staining could be another useful strategy for BP diagnosis, especially when DIF cannot be performed. In addition, we suggest that additional IHC staining of FFPE tissue may be helpful in cases of clinicopathologically suspicious BP with negative or suboptimal DIF results, instead of conducting a second biopsy.

263 PRAME Expression in Melanocytic Lesions of the Nail

Ourania Parra¹, Konstantinos Linos¹, Shaofeng Yan¹

¹Dartmouth-Hitchcock Medical Center, Lebanon, NH

Disclosures: Ourania Parra: None; Konstantinos Linos: None; Shaofeng Yan: None

Background: PRAME (Preferred Antigen for Melanoma) is an antigen first discovered on the surface of T-cells in a patient with melanoma. Since then, PRAME expression by immunohistochemistry (IHC) has been evaluated in a variety of melanocytic tumors, however, data on nail melanocytic lesions are scarce. Subungual melanoma can be diagnostically challenging, especially in the early stages. We evaluated PRAME IHC to assess its potential for differentiating benign from malignant nail melanocytic proliferations.

Design: We conducted a retrospective search of pathology archives between 2009 and 2020 and identified 40 cases of nail melanocytic lesions (8 invasive melanomas, 10 melanomas in situ, 3 melanocytic nevi, 3 lentigos and 16 cases of melanocytic activation). Patients' clinical characteristics from medical records were documented. H&Es and PRAME IHC were reviewed by two board certified dermatopathologists independently. The extent of PRAME was evaluated as follows: 0 no staining, 1+ 1-25%, 2+ 26-50%, 3+ 51-75%, and 4+ >75%. Consensus had to be reached in 4 cases.

Results: The difference in PRAME expression in malignant and benign lesions was statistically significant (Fisher exact test, p<0.01). Among the 18 malignant lesions, 11 (61.1%) showed a 4+ staining score, 3 (16.7%) showed a 3+ score, 2 (11.1%) showed a 1+ score and 2 (11.1%) showed a 0 score. For the 22 benign lesions, 1 (0.05%) showed a 2+ score, 6 (27.3%) showed a 1+ score, and 15 (68.2%) showed a 0 score. When the positive cutoff value for malignancy was decreased from score 4+ to 3+, the sensitivity of PRAME IHC test increased from 61% to 78% while the specificity remained the same (100%) since all the benign lesions (22/22) were considered negative with both cut-offs.

Conclusions: PRAME serves as a relatively sensitive and highly specific marker in differentiating benign from malignant melanocytic proliferations of the nail. However, the difference in sensitivity when using different cutoff values is not negligible. Therefore, the correlation between morphology and PRAME expression is imperative in the evaluation of melanocytic lesions of the nail.

264 Novel Double Immunohistochemistry (CD34/SOX10) for the Detection of Lymphovascular Invasion in Cutaneous Melanoma. Clinical-pathological Evidence Emerging from a Routine Set

Costantino Ricci¹, Stefano Chillotti¹, Francesca Ambrosi², Angelo Corradini¹, Martina Lambertini¹, Emi Dika¹, Michelangelo Fiorentino², Barbara Melotti¹, Barbara Corti¹

¹S.Orsola-Malpighi Hospital, University of Bologna, Bologna, Italy, ²Maggiore Hospital, University of Bologna, Bologna, Italy

Disclosures: Costantino Ricci: None; Stefano Chillotti: None; Francesca Ambrosi: None; Angelo Corradini: None; Martina Lambertini: None; Emi Dika: None; Michelangelo Fiorentino: None; Barbara Corti: None

Background: Lymphovascular invasion (LVI) is an unfavorable prognostic factor in cutaneous melanoma (CM). Detection of LVI by hematoxylin and eosin (H&E) staining alone is about 0%-6%, but previous studies showed that immunohistochemistry (IHC) targeting lymphovascular structures (D2-40, CD34, D2-40/MITF1) increase the detection rate of LVI up to 38%. As SOX10 proved to be the most sensitive melanocytic marker and CD34 stains

not only lymphatic but also vascular structures (“panvascular” marker), we decided to test double immunostaining for CD34/SOX10 in a routine set encompassing early and advanced-stage CM.

Design: Five authors independently evaluated 42 consecutive and prospectively enrolled cases of CM. We compared the LVI assessment with H&E and CD34/SOX10, analyzing the association with other clinical-pathological features (Chi-square and Fisher’s exact tests for dichotomous and categorical data; Kruskal-Wallis for continuous ones) and the interobserver agreement (Fleiss’s Kappa/FK and intraclass correlation coefficient/ICC).

Results: LVI was detected in 4 (9.5%) and 13 (31%) with H&E and IHC, respectively (McNamar=0.004). LVI detected by H&E stain was significantly associated with higher pT stage (2 pT2a and 2 pT4b; p=0.01) and Breslow thickness (p=0.013); conversely, LVI detected with IHC was not significantly associated with any clinical-pathological features. The interobserver agreement in LVI detection was higher with H&E (KF=0.561; ICC=0.869) compared to IHC (KF=0.490; ICC=0.833). Interestingly, no pT1a cases showed LVI with H&E whereas 5/42 (11.9%) ones showed LVI with IHC.

Conclusions: Our study showed that the IHC greatly increases the detection rate of LVI in a routine set of CM, but also how H&E-detected LVI is significantly associated with adverse clinical-pathologic features (pT stage and Breslow thickness) and improves the interobserver agreement. These results are particularly relevant because prove as the IHC applied to a routine set could probably lead to an overdiagnosis of LVI and overtreatment of the patients, especially for pT1a ones. Future studies are needed to investigate the correlation with survival data and to clarify the prognostic implications of cases with discordance between H&E and IHC.

265 Phenotypic Switch in Mycosis Fungoides: A Tertiary Cancer Center Experience

Shira Ronen¹, Jonathan Curry², Priya Nagarajan², Phyu Aung², Doina Ivan², Victor Prieto², Carlos Torres-Cabala², Michael Tetzlaff³

¹Cleveland Clinic, Cleveland, OH, ²The University of Texas MD Anderson Cancer Center, Houston, TX, ³University of California San Francisco, San Francisco, CA

Disclosures: Shira Ronen: None; Jonathan Curry: None; Priya Nagarajan: None; Phyu Aung: None; Doina Ivan: None; Victor Prieto: None; Carlos Torres-Cabala: None; Michael Tetzlaff: None

Background: Changes in immunophenotype in mycosis fungoides (MF) represent an uncommon phenomenon and may pose a significant diagnostic challenge. In the current study, we characterize this phenomenon further, both pathologically and clinically, by evaluating a large series of MF patients.

Design: MF cases with phenotypic switch (PS) between 2010-2020 were identified from pathology archives. Clinical data and follow-up information were obtained, and histopathological features were evaluated.

Results: Fifty-three biopsies displaying PS from 32 patients were identified (Table 1), including 13 women and 19 men with a median (mdn) age of 67.5 (range 17-89 years [y]). Figures 1&2 show PS in a case of CD4+/CD8- MF; a month later, a biopsy from a different anatomic location showed a CD4-/CD8+ phenotype, with partial loss of CD3. Fifteen patients (46.8%) had more than one PS during their disease course. Among those, two patients had two different PS on biopsies performed at the same time on different anatomic locations; CD4+ to CD8+ and CD4-/CD8- phenotypes; and CD8+ to CD4+ and CD4-/CD8- phenotypes. Time range for PS occurrence varied from 1 to 197 months [m] (mdn of 22 m) from the initial diagnosis. In 5 cases, identical TCR clone peaks were detected in the immunophenotypically distinctive lesions. No definite association between therapy and PS was observed. Follow-up ranged from 13 days to 165 m (mdn of 14.5 m). Thirteen patients died between 1.5 to 100 m (mdn of 14.2 m) after PS. Among the patients who died, the mdn time from MF diagnosis to the PS was 20.6 m (mdn age is 75 y), and among the patients that were alive, the mdn time was 44.1 m (mdn age is 66 y).

Table 1: Distribution of mycosis fungoides cases showing phenotypic switch

Phenotypic switch	Number of switches	Number of patients who died	Median time from diagnosis to phenotypic switch (months)
CD4+ to CD4-/CD8-	14	6 (42.8%)	41
CD4+ to subpopulation CD4-/CD8-	5	2 (40%)	12
CD4+ to CD8+	13	6 (46.1%)	50
CD4-/CD8- to CD4+	8	2 (25%)	43
Subpopulation CD4-/CD8- to CD4+	4	1 (25%)	26
CD8+ to CD4-/CD8-	6	4 (66.6%)	28
CD8+ to CD4+	5	1 (20%)	17
CD4-/CD8- to CD8+	4	4 (100%)	72
CD3- to CD3+	2	0	42
CD3+to CD3-	1	0	32

Figure 1 - 265

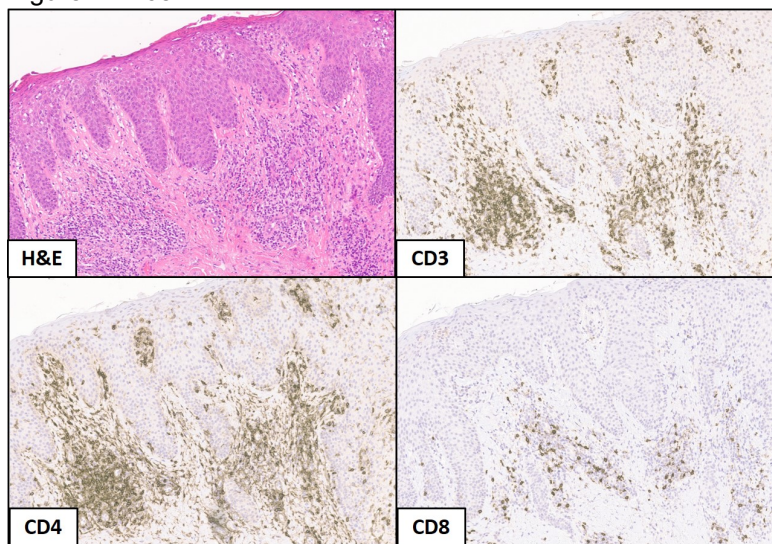
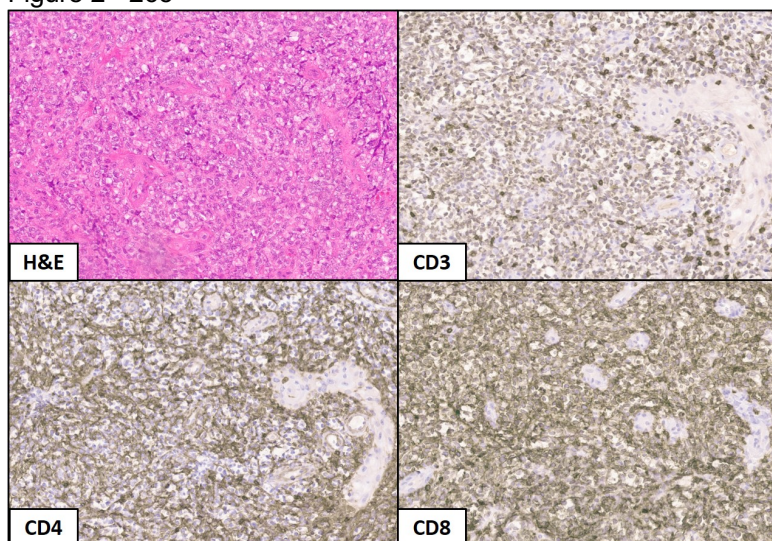


Figure 2 - 265



Conclusions: This represents the largest series of MF cases showing PS to date. This phenomenon may be not as rare as previously thought. No obvious association between PS and initiation or response to therapy was identified. 46.8% of cases displayed more than one PS suggesting that this phenomenon may occur temporally and anatomically distinctly during disease progression. Features that appeared to portend a worse clinical course were earlier PS in the course of the disease and specific PS from CD4-/CD8- to CD8+, and CD8+ to CD4-/CD8-. Awareness of this phenomenon is crucial to avoid misdiagnoses of second primary lymphomas and to alert the treating clinicians of potential changes in the clinical course of the disease.

266 Superficial Low-Grade Fibromyxoid Sarcoma

Shira Ronen¹, Jennifer Ko¹, Brian Rubin¹, Scott Kilpatrick¹, Wei-Lien (Billy) Wang², Alexander Lazar², John Goldblum¹, Steven Billings³

¹Cleveland Clinic, Cleveland, OH, ²The University of Texas MD Anderson Cancer Center, Houston, TX, ³Cleveland Clinic, Lerner College of Medicine, Cleveland, OH

Disclosures: Shira Ronen: None; Jennifer Ko: None; Brian Rubin: None; Scott Kilpatrick: None; Wei-Lien (Billy) Wang: None; Alexander Lazar: None; John Goldblum: None; Steven Billings: None

Background: Low-grade fibromyxoid sarcoma (LGFMS) is a distinctive spindle cell sarcoma that typically involves deep soft tissue (beneath the fascia) of the proximal extremities and trunk. Long-term follow-up has have shown a high rate of recurrence, metastasis, and death due to tumor. There is only one previous large series focusing on superficial LGFMS that suggested superficial tumors were disproportionately more common in children and may have a better prognosis. This study's primary goals are to confirm these findings and increase general awareness that LGFMS can arise in superficial soft tissue.

Design: The electronic surgical pathology file was queried at the authors' institutions to retrieve all cases of superficial LGFMS diagnosed between 2008 -2020. Superficial tumor location was confirmed for inclusion (23 cases). Available slides were reviewed, and clinical data and follow-up information were obtained.

Results: The clinicopathologic features are summarized in Table 1. Patients (9M;14F) had a median age of 29 years (range 2-65 years); 8 (34.8%) were children (<18 years), and 5 (21.7%) were young adults (18-30 years). The majority of the tumors were located in the lower half of the body (87%). The tumors were primarily centered in the subcutis (20; 87%, Fig. 1A), with 3 centered in the dermis (13%). They were circumscribed (95%) and had typical features of LGFMS with alternating fibrous and myxoid zones composed of bland, slightly hyperchromatic spindled cells (Fig. 1B). Necrosis was typically absent (96%), as was mitotic activity (83%). All were positive for MUC4 by immunohistochemistry (Fig. 1C) or *FUS* rearrangement by FISH. Follow-up on 11 cases ranged from 11.3 to 133.7 months (median 30.2 months) with no evidence of recurrence.

Table 1: Clinicopathologic Data on Superficial LGFMS

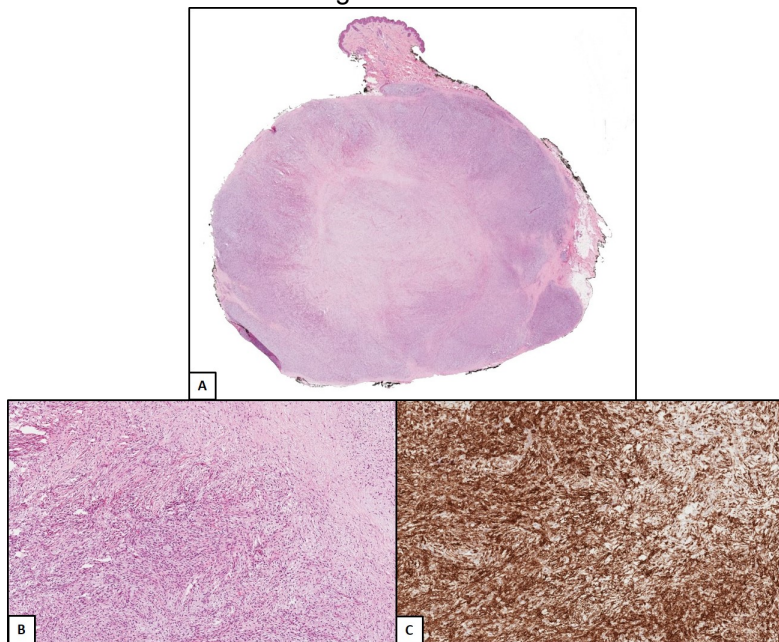
F, female; HPF, high power field; LTF, lost to follow-up; M, male; mo, months; NED, no evidence of disease; NI, not identified; y, years.

*Confirmatory test by MUC4 immunohistochemistry or FISH for *FUS* rearrangement.

Case No.	Age (y)/Sex	Site	Size (cm)	Location of tumor	Necrosis	Mitotic figures	Circumscribed/ infiltrative	Confirmatory test*	Follow-up (mo)	Outcome
1	52/M	Inguinal region	2.7	Subcutis	NI	NI	Circumscribed	<i>FUS</i> FISH	LTF	LTF
2	7/F	Thigh at inguinal crease	2.4	Subcutis	NI	1/10 HPF	Circumscribed	<i>FUS</i> FISH	133.7	NED
3	45/M	Abdominal wall	9.2	Subcutis	NI	NI	Circumscribed	<i>FUS</i> FISH	94.2	NED
4	4/F	Flank	2	Subcutis	NI	1/10 HPF	Circumscribed	<i>FUS</i> FISH	LTF	LTF
5	23/F	Groin	Unknown	Subcutis	NI	NI	Circumscribed	<i>FUS</i> FISH	LTF	LTF

6	46/M	Perianal	2.8	Dermis	NI	NI	Circumscribed	MUC4 IHC and <i>FUS</i> FISH	LTF	LTF
7	41/F	Leg	1.8	Subcutis	NI	1/10 HPF	Circumscribed	MUC4 IHC	LTF	LTF
8	57/F	Buttock	3	Subcutis	NI	NI	Circumscribed	MUC4 IHC	LTF	LTF
9	19/F	Axilla	1	Dermis	NI	NI	Circumscribed	MUC4 IHC	LTF	LTF
10	56/M	Buttock	4	Subcutis	NI	NI	Cannot be assessed	MUC4 IHC	LTF	LTF
11	61/F	Gluteal region	4.5	Subcutis	NI	NI	Circumscribed	MUC4 IHC	13.9	NED
12	12/F	Pretibial	3.3	Subcutis	NI	NI	Circumscribed	MUC4 IHC	40	NED
13	4/F	Gluteal region	2	Subcutis	NI	NI	Circumscribed	MUC4 IHC	11.3	NED
14	7/M	Thigh	2.8	Subcutis	NI	NI	Cannot assess	MUC4 IHC and <i>FUS</i> FISH	38.4	NED
15	29/M	Flank	4.2	Subcutis	NI	NI	Circumscribed	MUC4 IHC	30.3	NED
16	15/F	Thigh	1.6	Subcutis	NI	NI	Circumscribed	MUC4 IHC	LTF	LTF
17	29/M	Paraspinal	5	Subcutis	NI	NI	Infiltrative	MUC4 IHC	30.2	NED
18	50/M	Flank	5	Subcutis	Focal	NI	Cannot be assessed	MUC4 IHC	LTF	LTF
19	2/M	Great toe	1	Dermis	NI	NI	Circumscribed	MUC4 IHC	13.3	NED
20	23/F	Occipital scalp	2	Subcutis	NI	NI	Circumscribed	MUC4 IHC	LTF	LTF
21	8/F	Occipital scalp	Unknown	Subcutis	NI	1/10 HPF	Cannot be assessed	MUC4 IHC	LTF	LTF
22	65/F	Thigh	5	Subcutis	NI	NI	Cannot be assessed	<i>FUS</i> FISH	15.7	Death unrelated to LGFMS
23	49/F	Groin	3	Subcutis	NI	NI	Circumscribed	<i>FUS</i> FISH	61.9	NED

Figure 1 - 266



Conclusions: Superficial LGFMS affects children and young adults (56.5%) at a higher rate and may have a better prognosis than that for deep LGFMS. The largest limitation of our study is that many of our patients were lost to follow-up and that follow-up was somewhat limited. For that reason, further studies with longer follow-up would help support these findings.

267 Robust Classification of Melanocytic Lesions Using Deep Neural Networks: Flagging Dysplastic and Malignant Morphologies Before Pathology Review

Wonwoo Shon¹, Julianna Ianni², Bonnie Balzer¹, Saul Kohn², Ramchandra Vikas Chamarthi², Kameswari Devi Ayyagari², Sivaramakrishnan Sankarapandian², Rajath Soans², Mike Bonham²

¹Cedars-Sinai Medical Center, Los Angeles, CA, ²Proscia Inc, Philadelphia, PA

Disclosures: Wonwoo Shon: None; Julianna Ianni: *Employee*, Proscia Inc; Bonnie Balzer: None; Saul Kohn: *Employee*, Proscia, Inc.; Ramchandra Vikas Chamarthi: *Employee*, Proscia Inc; Kameswari Devi Ayyagari: *Employee*, Proscia Inc; Sivaramakrishnan Sankarapandian: *Employee*, Proscia Inc; Rajath Soans: None; Mike Bonham: *Employee*, Proscia

Background: While melanoma accounts for roughly 1% of annual skin cancer diagnoses, it is responsible for the majority of skin cancer deaths, with a survival rate for patients with metastatic melanoma at 20%. Of the over 2 million biopsies for melanoma each year in the US, approximately 15% are discordant or indeterminate, adding delay and uncertainty to diagnosis and complicating the treatment for these patients. In this work, we present a deep neural network trained to detect melanoma in unannotated whole slide images (WSIs) of Hematoxylin and Eosin stained histopathology specimens.

Design: Our training dataset consisted of WSIs from 1796 melanocytic biopsy and resection specimens from two laboratories with different scanners. No WSIs were excluded based on image quality or artifacts. Using a multiple-instance learning training criterion, a neural network learned to classify specimens based on an M score of 0-1 (<0.4 likely benign (LB), 0.4-0.9 suspect (S), >0.9 likely malignant (LM)). We evaluated the algorithm on an independent test set of 215 melanocytic biopsy and resection specimens: 125 melanomas (69 invasive and 56 in situ) 62 benign nevi, 28 dysplastic nevi (18 low-grade and 10 high-grade), No melanoma subtypes were excluded.

Results: Our model was able to distinguish between conventional nevi vs melanomas (AUC = 0.97) and dysplastic nevi vs melanomas (AUC = 0.92). 122/125 (98% sens) melanomas were flagged (90 LM and 32 S). Among dysplastic nevi, 16/28 (57%) cases were flagged as LM (1 high-grade and 1 low-grade) or S (8 high-grade and 6 low-grade). 54/62 (87%) benign nevi were LB; of note, 6 cases were flagged as S and 1 was LM.

Conclusions: Our deep learning based model accurately classifies a wide range of melanocytic specimens into actionable groups prior to pathology review. It could be used to prioritizing or triage cases within a digital workflow to increase laboratory efficiency. Alternatively, the model could flag discordant specimens for additional review, potentially improving diagnostic quality.

268 Differential Expression of Delta-like Protein 3 in Merkel Cell Carcinoma Primary Tumors and Metastases: A Novel Potential Therapeutic Target

Chauncey Syposs¹, Anthony Cardillo², Alexandra Danakas¹, Tatsiana Pukhalskaya², Bruce Smoller³, Tanupriya Agrawal¹

¹University of Rochester Medical Center, Rochester, NY, ²URMC Surgical Pathology Dept, Rochester, NY, ³University of Rochester School of Medicine and Dentistry, Rochester, NY

Disclosures: Chauncey Syposs: None; Anthony Cardillo: None; Alexandra Danakas: None; Tatsiana Pukhalskaya: None; Bruce Smoller: None; Tanupriya Agrawal: None

Background: Merkel cell carcinomas (MCC) are rare malignancies, with an estimated incidence of 470 cases per year in the United States. They are cutaneous neuroendocrine carcinomas associated with high rates of recurrence, metastasis, and poor overall survival. Delta-like Protein 3 (DLL3) is an inhibitory Notch ligand that is currently being developed as a predictive biomarker and potential therapeutic target for neuroendocrine carcinomas. While DLL3 is extensively studied in Small Cell Carcinomas of the lung, current literature on DLL3 expression in Merkel Cell carcinoma is sparse. In this study we analyzed the expression of DLL3 in primary cutaneous tumors and compared the expression to lymph nodes and distant metastases.

Design: We queried Merkel cell carcinoma cases diagnosed from 2012 – 2020 at the University at Rochester Medical Center. Cases were grouped based on whether the patient had a skin primary with no nodal or metastatic

disease (18 cases), metastatic Merkel Cell carcinoma identified in a lymph node (15 cases), and distant metastatic disease (10 cases). Patient history and microscopic slides were reviewed for each case to confirm the diagnosis of Merkel cell carcinoma. Cases deemed eligible were stained for DLL3 and INSM1 (a sensitive and specific nuclear marker of neuroendocrine carcinomas) and graded based on the percent of cells demonstrating membranous staining of DLL3 (no expression, <50% expression, >50% expression).

Results: DLL3 expression was observed in 89% (33/37) of cases. Our findings demonstrated an increased frequency of high expression of DLL3 in Merkel cell metastases (14 of 23; 61%) versus skin primary tumors (11 of 28; 39%) (Table 1A). We also compared DLL3 expression in ten cases with matched primary skin tumors, lymph nodes, and distant metastatic tissue, which demonstrated an increase in the frequency of high DLL3 expression in lymph nodes and distant metastases (14 of 23; 61%) versus their original primary skin tumors (4 of 10; 40%) (Table 1B).

Table 1A: DLL3 expression in Primary Skin Tumors versus Metastatic Tissue					
Skin Primaries			Metastatic Tissue		
No Expression	Low	High	No Expression	Low	High
3 of 28	14 of 28	11 of 28	1 of 23	8 of 23	14 of 23
0.11	0.50	0.39	0.04	0.35	0.61

Table 1B: DLL3 expression in Skin Primaries and their Metastatic Components					
Skin from Primaries with Metastasis			Distant Metastases and Lymph Nodes		
No Expression	Low	High	No Expression	Low	High
1 of 10	5 of 10	4 of 10	1 of 23	8 of 23	14 of 23
0.10	0.50	0.40	0.04	0.35	0.61

Figure 1 - 268

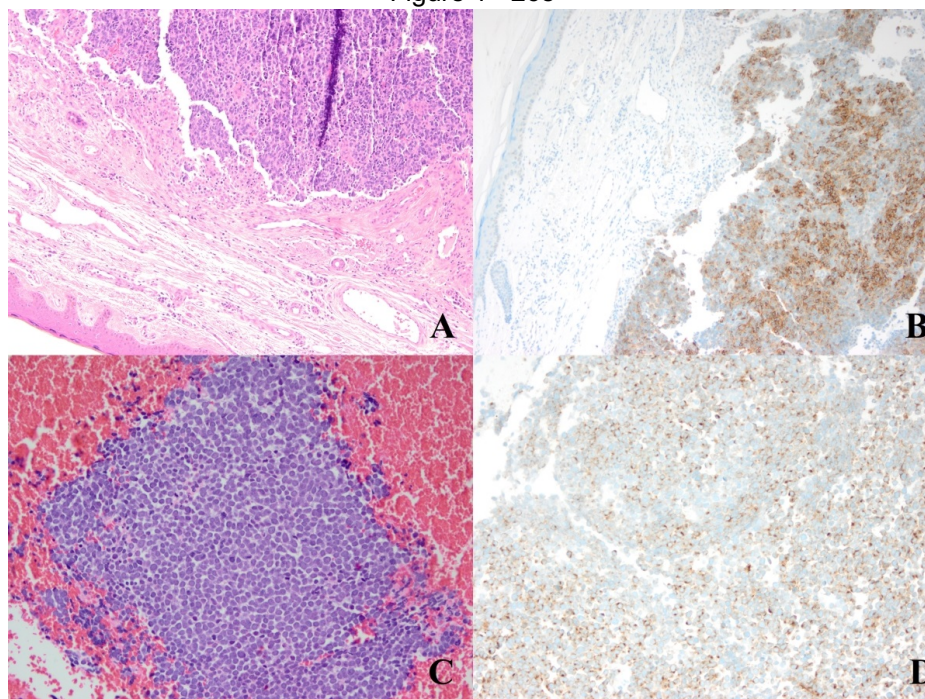


Figure 1: (A) Merkel cell carcinoma in a skin primary and (B) corresponding DLL3 staining from a patient with isolated cutaneous disease. This staining pattern was interpreted as expression >50%, high intensity. Panel (C) demonstrates metastatic Merkel cell carcinoma of the pancreas obtained through FNA, with the corresponding DLL3 (D) immunohistochemistry. This pattern was interpreted as >50%, low intensity.

Conclusions: Our study shows the expression of DLL3 in nearly all Merkel Cell carcinoma cases studied, suggesting a role for novel anti-DLL3 targeted drugs as a potential therapeutic option. Our results provide new insights into the differential expression of DLL3 in primary vs metastatic Merkel cell carcinoma. Further studies are required to explore the role of DLL3 plays in primary and metastatic Merkel cell carcinomas.

269 Molecular Profiling of Cutaneous C-Group Non-Langerhans Cell Histiocytoses

Rebekah Wieland¹, Tomas Bencomo², Carolyn Lee¹, Ryanne Brown¹

¹Stanford Medicine/Stanford University, Stanford, CA, ²Stanford University, Stanford, CA

Disclosures: Rebekah Wieland: None; Tomas Bencomo: None; Carolyn Lee: None; Ryanne Brown: None

Background: The 2016 revised classification of the histiocytoses consolidated and simplified new insights into this poorly-understood category of neoplasms; however, novel molecular findings with therapeutic relevance and new systemic associations continue to emerge, requiring continual refinement of our understanding of the cutaneous histiocytoses. A subset of the L-Group histiocytoses, specifically Langerhans cell histiocytosis (LCH) and Erdheim-Chester disease (ECD), have been extensively characterized with the majority of cases showing abnormalities in the Ras/Raf/MEK/ERK pathway resulting in MAPK signaling activation. The R-Group, consisting of Rosai-Dorfman disease and its variants, can also show Ras/Raf/MEK/ERK pathway mutations, similar to the L-Group. While L-Group and R-Group histiocytoses have been extensively characterized, the C-Group histiocytoses have not been molecularly profiled outside of the setting of isolated case reports.

Design: 13 cutaneous C-group non-Langerhans cell histiocytoses were collected retrospectively from the pathology archives after IRB approval. Tumor was microdissected from formalin-fixed, paraffin embedded tissue. Whole genome sequencing was performed with an average depth of 25X and somatic variants were detected using Mutect2. Variants were annotated using the Ensembl Variant Effect Predictor and Combined Annotation Dependent Depletion (CADD) deleteriousness score.

Results: Recurrent hotspot missense and splice site mutations with high CADD scores were identified in *KMT2B* (p.E1034A) in 5/13 cases (38%), *HGH1* (p.G54V) in 3/13 cases (23%), *AC239859.5* (splice site) in 2/13 cases (15%), *GTPBP6* (p.G61R) 7/13 cases (54%), *ZBED3* (p.L155A) in 5/13 cases (38%), *MUC5AC* (p.P1919L) in 3/13 cases (23%), and *SYN2* (p.P105A) in 3/13 cases (23%). Ras/Raf/MEK/ERK pathway mutations were observed in 2/13 cases (15%).

Conclusions: This is the first and largest series to perform whole genome sequencing on cutaneous C-group non-Langerhans cell histiocytoses. Our data support the finding of recurrent deleterious missense and splice site mutations in this group. We are currently examining structural variants within this cohort.

270 MicroRNA Expression Signature Differentiates Primary Lentiginous from Non-Lentiginous Acral Melanoma

Richard Yang¹, Shira Ronen², Achim Bell¹, Priya Nagarajan¹, Jonathan Curry¹, Doina Ivan¹, Victor Prieto¹, Carlos Torres-Cabala¹, Phyu Aung¹

¹The University of Texas MD Anderson Cancer Center, Houston, TX, ²Cleveland Clinic, Cleveland, OH

Disclosures: Richard Yang: None; Shira Ronen: None; Priya Nagarajan: None; Jonathan Curry: None; Doina Ivan: None; Victor Prieto: None; Carlos Torres-Cabala: None; Phyu Aung: None

Background: Primary acral lentiginous melanoma (PALM) is a melanoma that commonly arises on the volar skin of the soles, palms, digits, and nail apparatus. Unlike most subtypes of melanoma, PALM is thought not to be driven by chronic sun exposure. It occurs relatively more commonly in patients of African, Asian, and Latin ethnicity. Interestingly, somatic mutations in the RAS pathway have been described in 87% of these neoplasms, a unique pathogenesis uncommonly seen in non-lentiginous type melanomas from acral sites (NALMs). Due to this difference in pathogenesis, we sought to determine the differential miRNA expression levels between PALM and NALMs.

Design: Melanocytic lesions from 23 patients (Table 1) were macrodissected (10 PALM, 6 NALMs, and 8 nevi) to isolate lesional cells. The differentially expressed microRNAs (miRNAs) were analyzed using the Nanostring Human microRNA v3 panel, including 837 probes, including 827 human miRNA probes, and targeting 665 unique human miRNAs. Normalization and analysis, including hierarchical clustering and graphical representations, were performed using the Nanostring nSolver software (version 4.0) and Functional Annotation (FA) Tool using the online resource, DAVID Bioinformatics Resources 6.8, NIAID/NIH. GraphPad Prism v8.4.3 was used to create Kaplan Meier survival curves and performed survival analysis.

Results: Differential expression between 16 melanomas and 8 nevi yielded a set of 14 probes with False Discovery Rate (FDR) < 0.25: *miR29A*, *miR21*, *miR4286*, *miR16-1*, *miR15B*, *miR150*, *miR222*, *miR1180*, *miR93*, *miR30D*, *miR1253*, *miR630*, *miR494*, and *miR29C* (Fig. 1A). FA of this miRNA set yielded the KEGG pathway “MicroRNAs in cancer” with a nominal p-value of 8.1×10^{-12} and Benjamini-Hochberg correction (FDR) of 1.6×10^{-11} . Differential expression analysis between PALM and NALM identified 17 miRNAs using p-value < 0.05 (*RPL19*, *ACTB*, *RPLP0*, *miRLET7B*, *miR181A2*, *miR191*, *miRLET7G*, *miR513B*, *miR361*, *miRLET7E*, *miR99B*, *miR340*, *miR497*, *miR199B*, *miR3065*, *miR551B*, and *miR610*, Fig. 1B). FA of this set identified enrichment for the “focal adhesion” Gene Ontology (GO) pathway with p-value: 4.6×10^{-4} and FDR: 1.2×10^{-2} . We also found relatively shorter metastasis free survival in patients with PALM compared to those with NALM in this cohort (p-value = 0.1079, Fig. 2).

Case	Age/Sex	Race	Clark level	Breslow thickness (mm)	Mitotic figures	Ulceration	Regression	LVI	PNI	Microscopic satellitosis	LN metastases
N1	24/M	White	-	-	-	-	-	-	-	-	-
N2	47/M	White	-	-	-	-	-	-	-	-	-
N3	34/F	White	-	-	-	-	-	-	-	-	-
N4	56/M	White	-	-	-	-	-	-	-	-	-
N5	64/M	White	-	-	-	-	-	-	-	-	-
N6	16/M	White	-	-	-	-	-	-	-	-	-
N7	32/M	White	-	-	-	-	-	-	-	-	-
N8	62/F	White	-	-	-	-	-	-	-	-	-
PALM1	78/M	White	5	>4	5-9	Yes	NI	Yes	NI	NI	0/3
PALM2	75/F	Hispanic	5	>4	5-9	NI	NI	Yes	Yes	Yes	2/17
PALM3	59/F	Unknown	5	>4	10-20	NI	Yes	NI	Yes	NI	4/4
PALM4	53/F	White	5	>4	1-4	NI	NI	Yes	Yes	NI	2/2
PALM5	83/F	White	4	2.04-4.04	5-9	Yes	NI	NI	NI	NI	1/2
PALM6	83/F	Hispanic	5	>4	1-4	NI	NI	Yes	Yes	Yes	2/2
PALM7	69/M	White	5	>4	>20	Yes	Yes	Yes	Yes	NI	2/2
PALM8	76/M	White	4	2.04-4.04	1-4	Yes	NI	NI	Yes	NI	0/2
PALM10	79/M	White	4	2.04-4.04	1-4	Yes	NI	NI	NI	NI	3/3
NALM1	36/M	African American	5	>4	1-4	NI	NI	Yes	Yes	NI	9/14
NALM2	58/F	White	5	0.8-1.04	10-20	Yes	NI	NI	NI	NI	5/8
NALM3	89/F	White	4	>2.04-4.04	1-4	NI	NI	NI	NI	NI	1/3
NALM4	2/F	White	5	>2.04-4.04	1-4	NI	NI	Yes	NI	NI	1/1
NALM5	86/M	White	4	1.04-2.04	1-4	NI	NI	NI	NI	NI	NP
NALM6	32/M	White	4	<0.8	0 or <1	NI	Yes	NI	NI	NI	NP

Table 1: Clinicopathological features; N: nevus; NALM: non-lentiginous type melanomas from acral sites; NI: not identified; NP: not preformed; PALM: Primary acral lentiginous melanoma

Figure 1 - 270

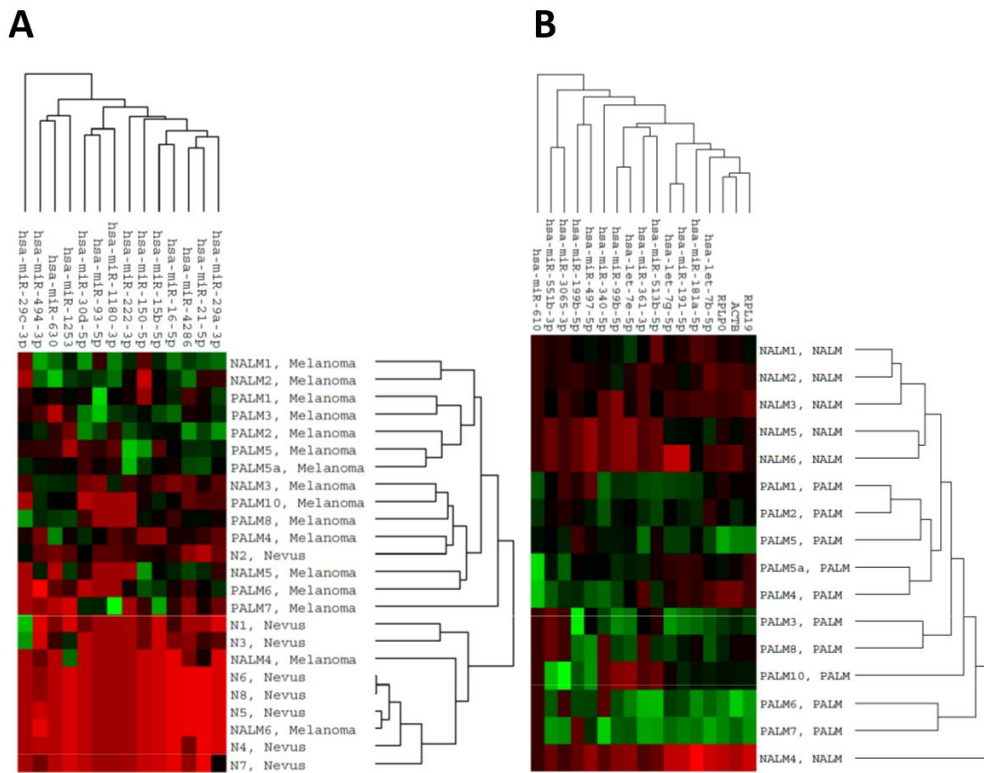


Figure 1. (A) MicroRNA Expression Signature Differentiates Acral Melanoma from Acral Nevus. (B) MicroRNA Expression Signature Differentiates Primary Acral Lentiginous Melanoma (PALM) from Non-Lentiginous Types Melanoma from Acral Sites (NALM).

Figure 2 - 270

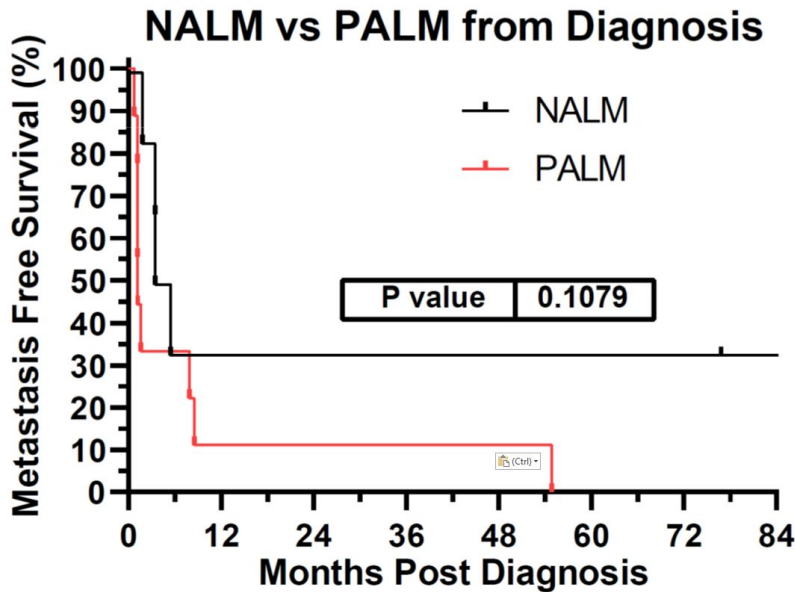


Figure 2. Kaplan Meier curve showing relatively shorter metastasis free survival in patients with PALM compared to those with NALM in this cohort.

Conclusions: Our findings suggest that miRNA-based expression signature differs among different types of acral melanocytic lesions (i.e., melanoma vs. nevus, and PALM vs. NALM). The results also highlight the potential role of some miRNAs in cell adhesion, a finding that may help explain the histological phenotype of PALM (characteristic confluent single cell proliferation / pagetoid spread) and worse prognosis compared to NALM.